Final Report

NASA CR-132265

FERRITE LOGIC RELIABILITY STUDY

By: JAMES A. BAER C. BRUCE CLARK

Prepared for:

NATIONAL AERONAUTICS AND SPACE ADMINISTRATION
LANGLEY RESEARCH CENTER
HAMPTON, VIRGINIA 23365

CONTRACT NAS 1-11453

STANFORD RESEARCH INSTITUTE
Menlo Park, California 94025 · U.S.A.

STANFORD RESEARCH INSTITUTE
Menlo Park, California 94025 · U.S.A.

Final Report

July 1973
NASA CR-132265

FERRITE LOGIC RELIABILITY STUDY

By: JAMES A. BAER C. BRUCE CLARK

Prepared for:

NATIONAL AERONAUTICS AND SPACE ADMINISTRATION
LANGLEY RESEARCH CENTER
HAMPTON, VIRGINIA 23365

CONTRACT NAS 1-11453

SRI Project 1832

Approved by:

FRED J. KAMPHOEFNER, *Director*
Engineering Sciences Laboratory

BONNAR COX, *Executive Director*
Information Science and Engineering Division

Copy No. .....

Page Intentionally Left B

CONTENTS

ILLUSTRATIONS

ACKNOWLEDGMENT

Significant contributions have been made to the success of this project by several individuals. David Nitzan has contributed to the investigations and has written a portion of this report. John Gill measured the magnetic characteristics of the devices and circuits, Thomas Drewek conducted the environmental testing and electrical measurements, and Dante Petro, Physical Sciences Division, carried out sample preparation and high magnification microscopy.

We also wish to acknowledge the cooperative attitude and actions of personnel from Ampex Research Department, Ampex Corporation, Redwood City, California.

I INTRODUCTION

There is a continuing need for increasing the reliability of digital electronic systems, especially in complex systems that are inaccessible and carry a high penalty for operational failure. NASA has recognized the need for increasing the reliability in aircraft and spacecraft electronic systems, and has supported appropriate research and development activities.

One method advanced to meet the need for higher reliability is to develop and use a class of digital circuits called "all-magnetic logic." In these circuits the magnetic elements and their windings comprise the active circuit devices in the logic portion of a system. (In the power supply to such a system, the clock-current generator may require semiconductors, vacuum tubes, etc.) The Ferrite Logic (FLO) device that was developed through NASA support belongs to the all-magnetic class of logic circuits. The FLO device is novel in that it makes use of a dual or bimaterial ferrite composition in one physical ceramic body. This bimaterial feature, coupled with its potential for relatively high speed operation, makes it attractive for high-reliability applications. (Maximum speed of operation approximately 50 kHz.)

The high reliability attributed to all-magnetic logic implementation of digital systems has been inferred from the reliability experience in computer memories using ferrite toroids, from other magnetic systems, and from the limited number of known failure modes for ferrite ceramics. While there appears to be wide acceptance of the reliability potential of magnetic systems, there is a need to assess their reliability, including interconnections, in a manner that will permit comparison with the more

conventional devices. The main purpose of this project has been to assess the reliability of the FLO device.

Magnetic devices have been shown to be relatively insensitive to nuclear radiation effects, and this study did not address the radiation sensitivity aspect of reliability.

II SUMMARY AND CONCLUSIONS

FLO devices are in developmental status in the methods, materials, and processes for fabrication of physical devices, as well as in the logic design aspects of system implementation. Because changes in the device per se are in progress in attempts to improve its performance, it is difficult to evaluate the reliability of the device, a circumstance that was recognized before the inception of this project. Similarly, it was recognized that only a limited number of test specimens would be available for evaluation. These two facts were considered, and it was concluded that it was worthwhile to make an assessment in spite of these difficulties.

The program included environmental testing, study of magnetic circuit operational parameters, prediction and study of failure modes, and physical examination of test specimens. A major factor determining the direction of our investigation, and the emphasis given to the several facets of the work, has been the formidable device-fabrication problems encountered by the developers during the period of this project. These fabrication problems led to considerable variability in characteristics from one test specimen to another, and these fabrication problems have spawned premature failures in test specimens. Unfortunately, it is not possible to somehow look beyond the current situation, postulate the reliability potential of the device, and then proceed with the reliability study by divorcing the study from the details of the fabrication process and manufacturing quality control procedures that are exercised during the fabrication of the device. What we have done, however, is study the nature and causes of failures in the test specimens.

Failures observed in the dielectric and conductor parts of the FLO device stem mainly from liquid chemical processes and exposure to high temperature during fabrication. In addition, adhesion of deposited conductors to dielectric surfaces needs improvement. Failures observed in the magnetic parts of the device result, at least in part, from cracks in the ferrite. There is evidence showing that the cracks occur during the formation of the ferrite rather than thereafter.

High reliability has not yet been achieved for the FLO device, and improvements in the processing procedures and/or a new fabrication approach are required in order to improve reliability to an acceptable level.

III MAGNETIC CIRCUIT OPERATING CHARACTERISTICS

A. Bimaterial Multipath Magnetic Device

The Ferrite Logic (FLO) devices studied in this project belong to a class of digital circuits called all-magnetic logic.* The active circuit elements in these circuits comprise magnetic flux paths and conducting electrical paths. As the name implies, there are no semiconductors or other devices in the logic portion of the circuit (however, there are active devices in the pulse current sources that supply the power). A FLO device can be further characterized as being a nonresistance type of all-magnetic logic scheme; it makes use of flux steering and has a novel, if not unique, bimaterial ferrite structure.

Figure 1 shows a multipath ferrite device that is the basic magnetic element in the magnetic circuit that is the concern of this study. This magnetic device is sometimes referred to as an Exclusive-OR structure. However, in the test specimens used in this reliability assessment, the logic function performed by this element is one of delay, i.e., one stage in a ring counter. The details of the development and operation of this multipath device are described elsewhere[2-4] so only the basic features will be discussed in this report.

An entire multipath (or multiaperture) device is made of square-loop ferrite ceramic material. A significant feature of this particular family of all-magnetic devices is that two ferrite compositions are formed into one physical device. One ferrite composition has a low coercive force and the other ferrite composition has a high coercive force. Forming the

---

*A bibliography of all-magnetic circuits is presented in Reference 1.

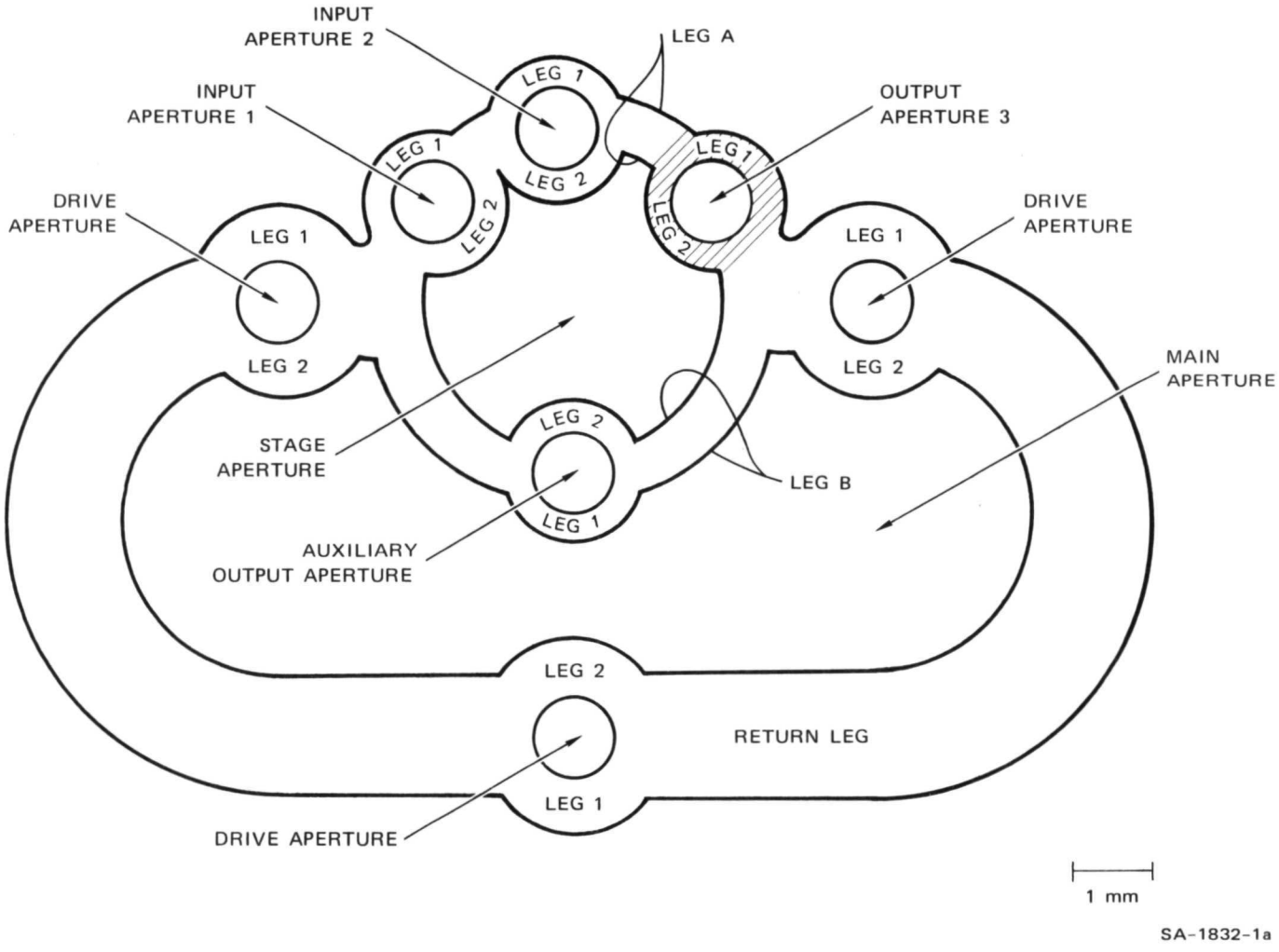

FIGURE 1a APERTURE AND LEG IDENTIFICATION FOR MULTIPATH FERRITE LOGIC DEVICE

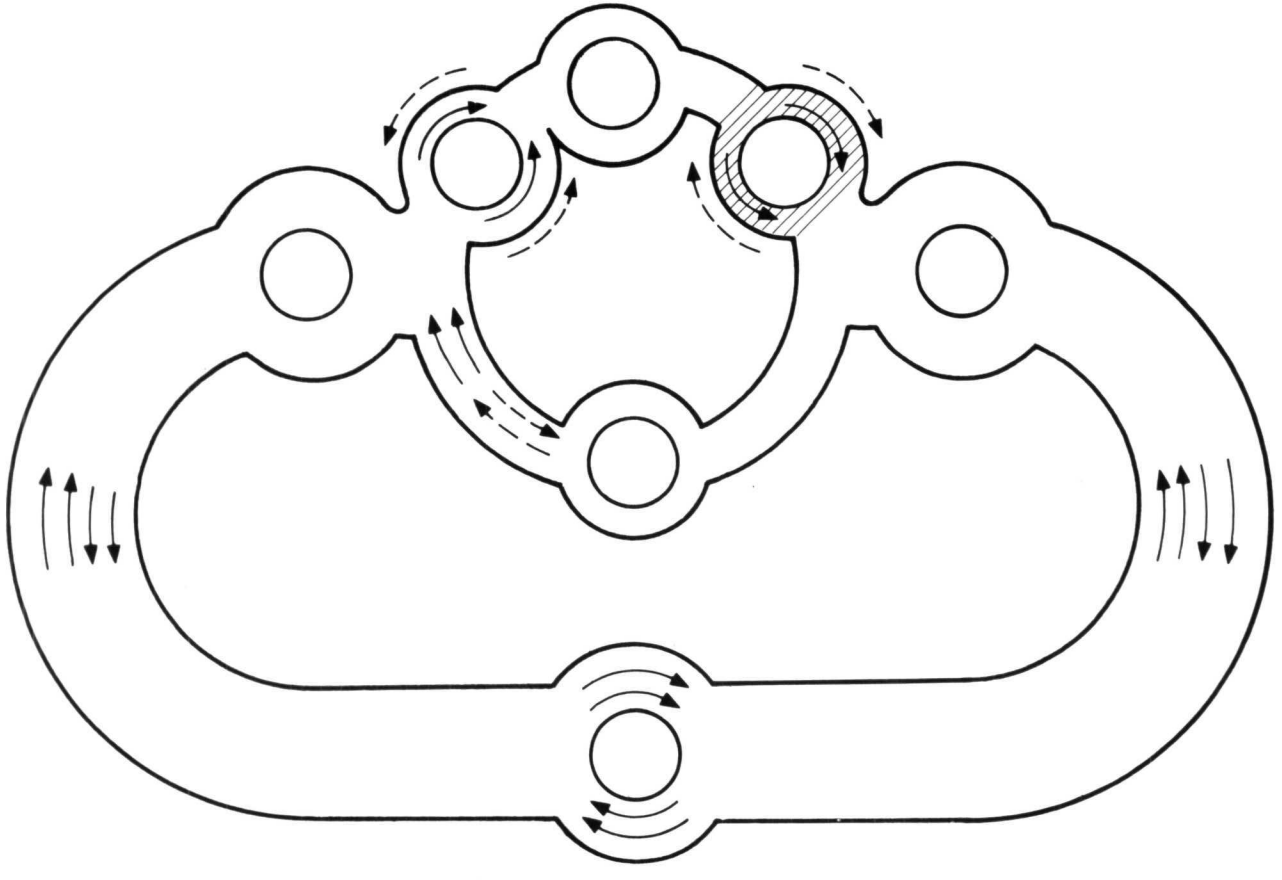

FIGURE 1b FLUX STATES AFTER TRANSFER FOR MULTIPATH FERRITE LOGIC DEVICE

two different compositions into one magnetic structure increases the operating range of the circuit; that is, increases the tolerance of the device to variations in current pulse amplitude and/or tolerance to ambient temperature variations. Referring to Figure 1A the low coercive force ferrite is used in a more or less toroidal region (shaded area in figure) surrounding the output aperture. The high coercive force material is used for all the remaining portions of the multipath magnetic device. Because the low coercive force material is around the output aperture, flux transfer from the output to another device requires a smaller drive current amplitude than would otherwise be true. Since the maximum allowable current amplitude is essentially unaffected by the value of the coercive force around the output aperture, the drive current amplitude tolerance of the device is increased.

Arrows in Figure 1B, within or adjacent to the various magnetic paths, indicate the direction of flux in that particular path. Each arrow represents one unit of flux, or nominally 100 nWb. The arrows in the return leg show two units clockwise and two units counterclockwise around the main aperture indicating a demagnetized state for this leg. When all four arrows are in the clockwise direction around the main aperture, the entire core is saturated and is said to be in the clear state.

In time sequence, the operation of the device proceeds as follows: Assume initially that the core is in the clear state. During the next clock phase, current through the three drive apertures puts the return leg in its demagnetized condition. If a ZERO is to be transferred into the core, the direction of the flux in Leg B is reversed and the direction of the flux in Leg A remains unchanged. This state is shown by solid arrows in the figure. During this ZERO transfer, flux is steered into Leg B preferentially by a bias current applied through the stage aperture. (This same current also links Leg 2 of the input aperture (#1) and a clipper core, which has not yet been discussed.) When a Logic ONE

is to be transferred into the multipath core, a steering current is applied to Leg 1 of the input aperture (#1) by means of a coupling loop winding. This current steers one unit of flux, i.e., one arrow, into Leg A in the counterclockwise direction. This unit of flux is steered away from Leg B. Therefore, the flux state after a ONE has been transferred is such that Leg A is demagnetized, Leg B is demagnetized and the return leg is demagnetized. This means that each aperture around the stage aperture is effectively decoupled from the remaining magnetic circuit. Note that the counterclockwise flux around the output aperture goes into Leg 2, rather than Leg 1. This is because the output coupling loop (not shown) effectively shorts out Leg 1 during this transfer.

After the core is put in either the ONE or ZERO state, a drive current is applied through the output aperture. In the case of the Logic ONE state, flux can switch locally around the output aperture as though it were an isolated toroid. In the Logic ZERO case, flux cannot switch locally around the aperture unless a high amplitude drive current is applied to unblock this portion of the core. Subsequent to applying a drive current to the output aperture and transferring either a ONE or a ZERO out of this core, the entire core is cleared by a multiturn winding through the main aperture which returns all flux around this aperture to the clockwise sense, the clear state.

The amount of remanent flux switched around three paths of the multipath device as a function of the applied pulse drive current amplitude is shown in Figure 2. In a qualitative sense, these curves can be viewed as portions of the normal type of BH loop. The figure shows only the part of the loop normally drawn in the first and fourth quadrants. The three curves shown as a solid line were all measured on the same device. The curves show that flux begins to switch around the output aperture at a much lower current level than is required for switching around the input aperture, in spite of the fact that the path lengths are identical. This

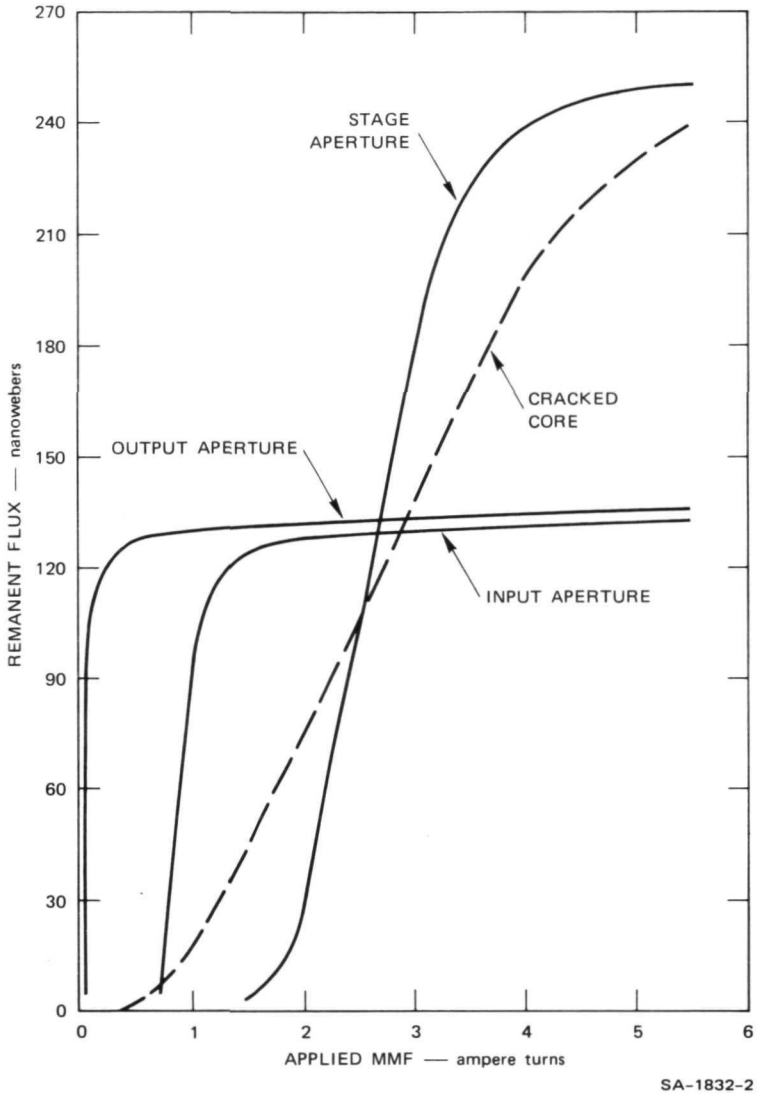

FIGURE 2 STATIC ϕ-F CHARACTERISTIC

demonstrates the effectiveness of using a bimaterial device with low coercive force material around the output aperture. The curve for the stage aperture shows that the threshold, or the amount of current required to initiate switching, is greater for this aperture than the other two. This is because of the increased path length. This curve also shows that the maximum flux that can be switched around the stage aperture is greater than for the other two apertures. This is due to the greater cross-sectional area of the path around the stage aperture. In the ideal case,

the maximum flux that can be switched around the stage aperture should be twice the amount around either the input or the output aperture. The input and output apertures should have equal maximum values.

The characteristic shown as a dashed line was measured around the stage aperture of a different test specimen and it indicates that a crack, or probably multiple cracks, are present in this magnetic path. The cracks cause air gaps in the magnetic circuit and result in shearing (tilting) of the loop.

B. Shift Register Stage

The connection of two multipath cores together in a fashion that makes one stage of a shift register (or two stages of a ring counter) is shown in a rudimentary fashion in Figure 3. This circuit was selected as the basis for this reliability study. The magnetic ferrite elements in this circuit comprise two Exclusive-OR structures and two toroids. The test specimens examined during this project were supplied without coupling loops at the input and output of the stage but with a coupling loop between the Odd and Even cores and a "set-in" winding in input aperture number two that provides connection to a laboratory pulser.

When flux is switched locally around the output aperture of the Odd core under the influence of a drive current (winding not shown), current is induced in the coupling loop that links a clipper core and the input aperture of the Even core. The clipper core functions as a flux sink that is necessary to cancel noise effects during ZERO transfer and shapes the flux gain curve. The flux gain curve, the amount of flux switched in one portion of a magnetic circuit compared to the amount switched in another portion, must have a prescribed shape and values in order to permit propagation of a binary signal from stage to stage. The detailed mechanisms of flux transfer are covered in References 1 and 5.

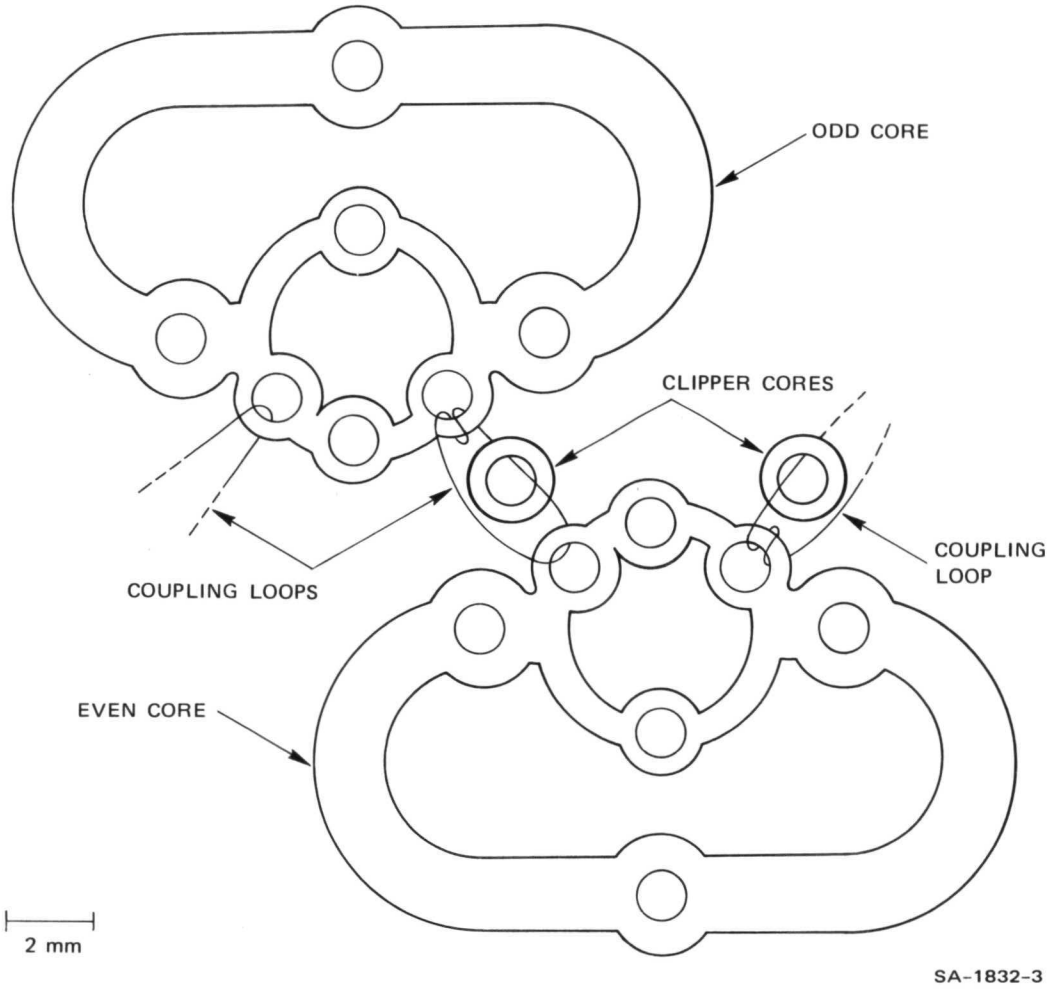

FIGURE 3 ONE STAGE OF A SHIFT REGISTER (DRIVE WINDINGS NOT SHOWN)

The flux gain characteristic that we measured on one test specimen is shown in Figure 4, where the abscissa represents the flux switched in the input aperture of the Odd core, and the ordinate represents the flux switched in the input aperture of the Even core. The dashed line at 45° represents unity flux transfer. Note that the shape of the curve for the flux transfer is like the letter S. It crosses the unity gain line at three points. The lower and upper crossing represent stable operating

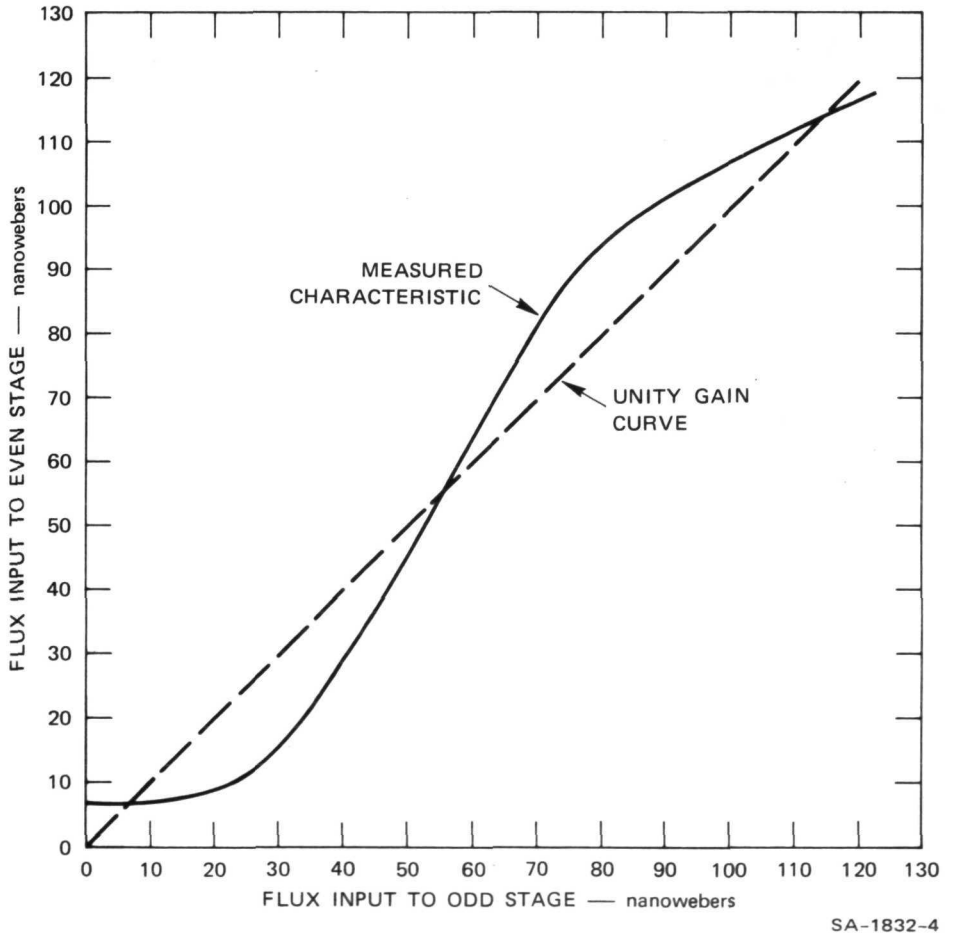

FIGURE 4 FLUX GAIN CHARACTERISTIC

points for binary flux transfer. It is essential for bistable operation that the curve have this shape and cross the unity gain line at three positions, as shown in this example. The square-loop characteristic of the ferrite material shown in Figure 2 and the flux gain characteristic shown in Figure 4 are both necessary characteristics for bistable device operation. These curves show that this essential feature can be achieved in the FLO device.

Figure 5 is a photograph of a test specimen like the ones used in this study. In the photograph, two ferrite cores (normally hidden) have been added to the test specimen to show more clearly the geometrical relationship between the cores themselves and the complex wiring pattern. As will be discussed shortly, all of these windings are fabricated by electroplating. The specimen shown has drive windings, which comprise the majority of the conductors pictured, and a coupling loop winding linking the Odd and Even cores. The photograph shows the specimen magnified about six times. The multipath ferrite core is approximately 1.0 by 1-1/2 cm.

Figures 6 and 7 are top and bottom views showing the identification numbers used to locate various parts of the test specimen. When a location number is cited, these two photographs can be used to identify the portion of the specimen to which reference is made. The photographs were taken of a specimen that was made during the early part of this project, and they represent the tube and conductor placements at that time. The placement was modified on specimens made at a later date. Drive windings and a single set-in winding at Locations 58 and 60 are pictured, but the coupling loop winding is omitted for clarity. In Figure 7, some of the set-in conductor strips are included as an aid in orientation. There are eight drive windings on each test specimen; four link the Odd core and four link the Even core. All drive windings have a common connection shown at the right side of Figure 6. In circuit operation, a separate

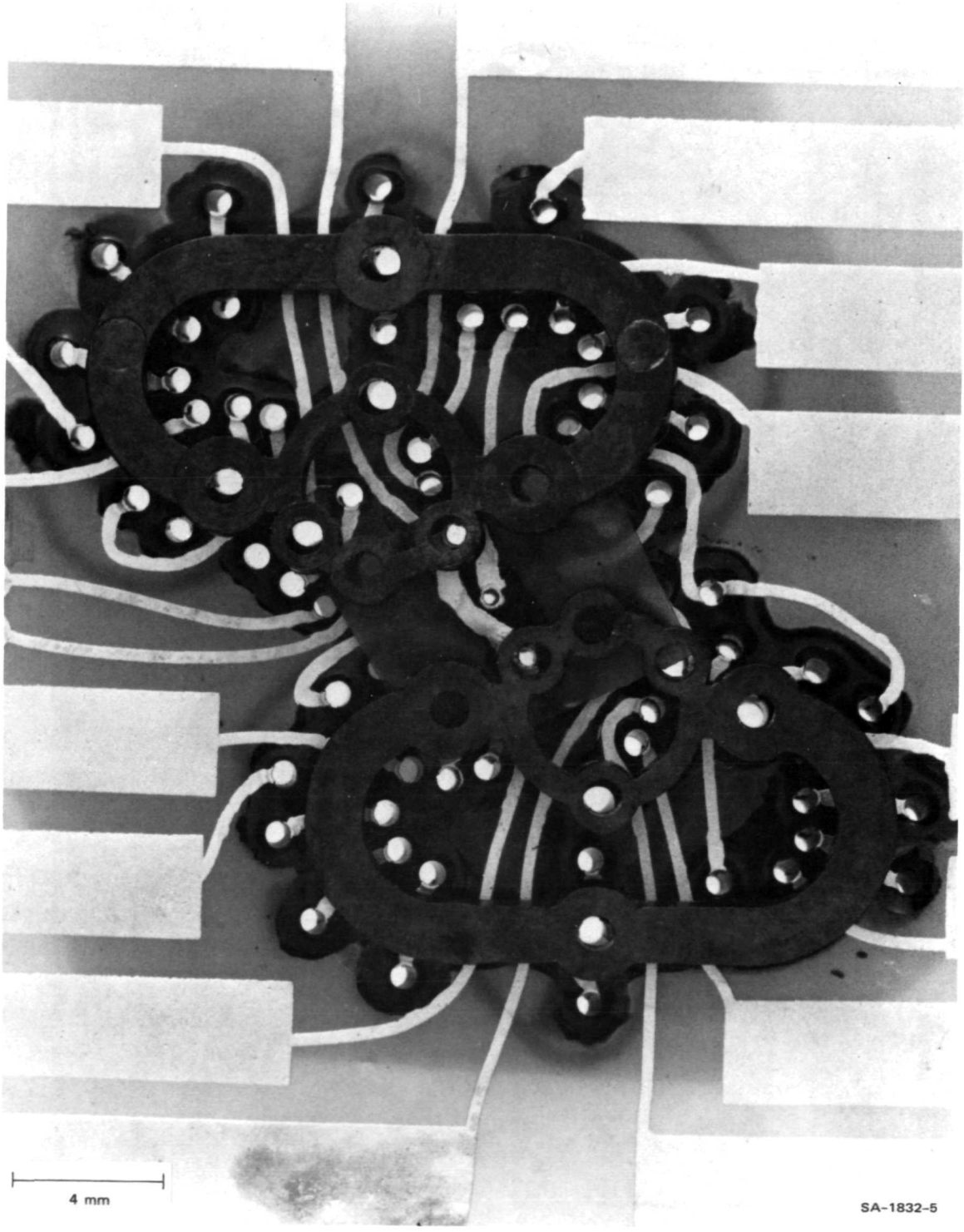

FIGURE 5 TEST SPECIMEN WITH FERRITE CORES SUPERIMPOSED

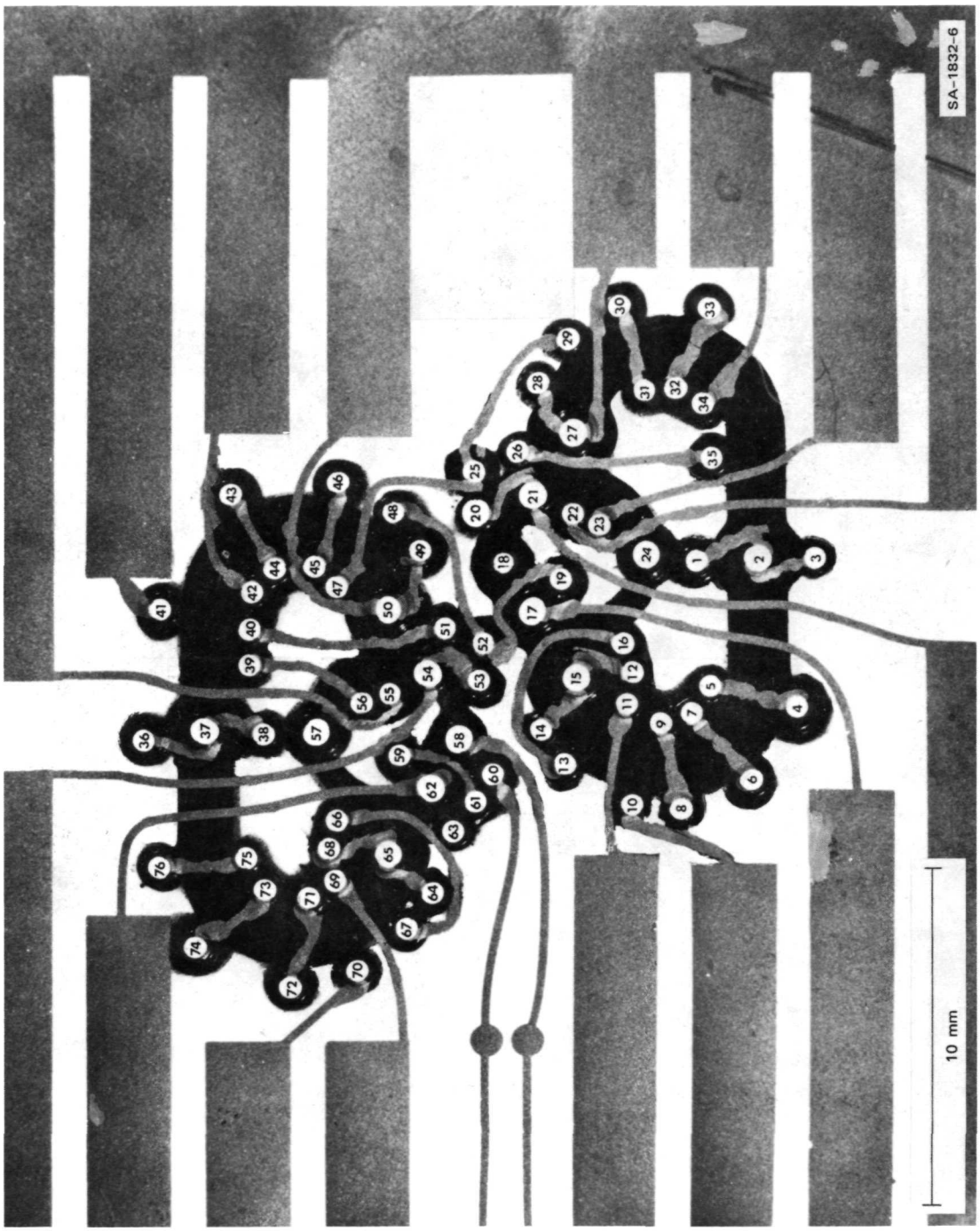

FIGURE 6 TOP VIEW WITH LOCATIONS IDENTIFIED

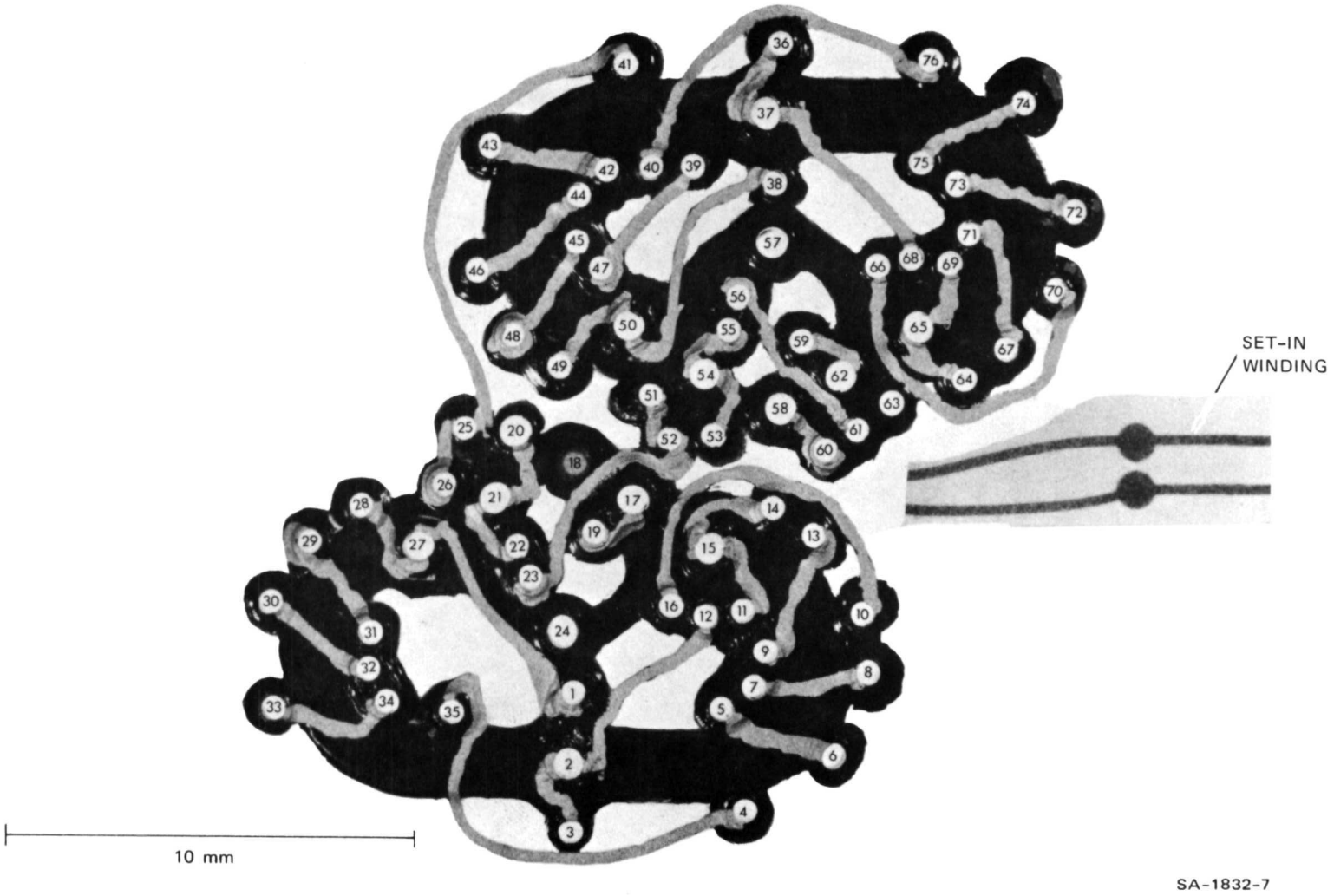

FIGURE 7 BOTTOM VIEW WITH LOCATIONS IDENTIFIED

pulse current source is connected to each of the eight windings shown on the left side of Figure 6.

IV DEVICE FABRICATION PROCEDURE

A. Plated Bimaterial Ferrite

The finished FLO device is a multilayer structure composed of several different materials. The largest physical elements in the entire structure are the pieces of ferrite. As discussed previously, the multipath ferrite piece is made up of two different ferrite compositions. To make this bimaterial ferrite, the two compositions are compression-bonded by applying heat and pressure simultaneously prior to sintering. The compositions at this point in the process are in the form of a suspension of ferrite binder and solvent formulated in flexible sheets.[6]

Figure 8 shows a photograph of the output aperture region of a polished specimen; the low coercive force material surrounds the aperture and extends into the adjacent regions. There are fewer voids in the low coercive force material than in the high coercive force material, but voids are normal for ceramic ferrites. The light and dark regions visible in the low coercive force material are grains or crystallites. The transition region between the two materials, visible in the photograph, has the appearance of a good mechanical bond. The white border strip is the plated copper eddy current shield that conforms to the outside of the ferrite. The shield on the inside-diameter surface of this specimen was omitted in later core samples to increase the space available for insulation and conductor segments. The aperture diameter is approximately 1 mm.

The copper shield is made by first applying a gold-bearing liquid (resinate)* directly to the ferrite and then curing it at 300°C. After

---

*Hanovia Squeegee Bright Gold #8119.

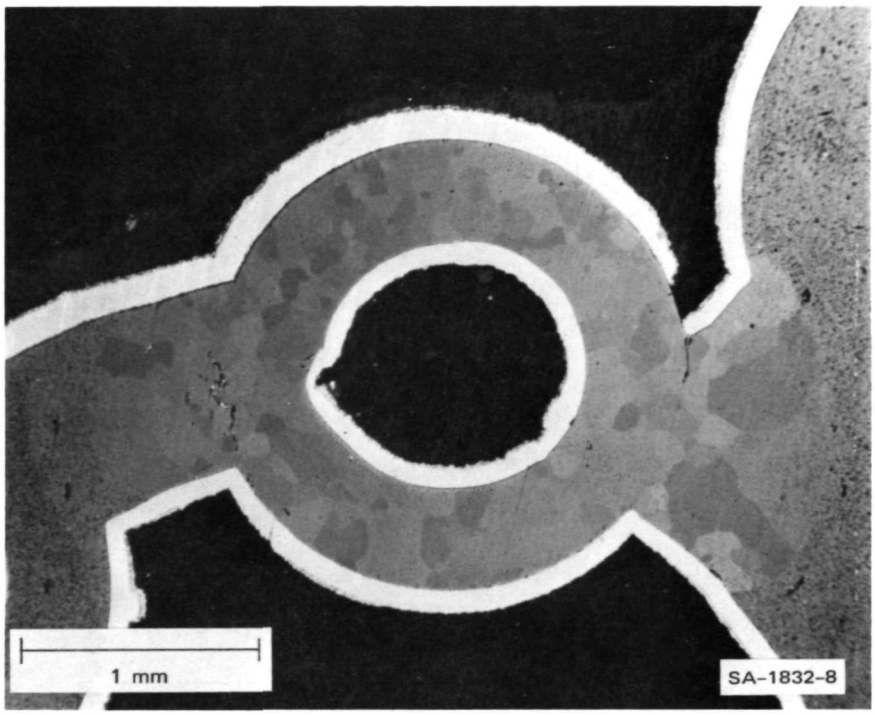

FIGURE 8 BIMATERIAL FERRITE OUTPUT APERTURE REGION AT 32X

curing, the thickness of the gold is increased by electroplating more gold, and the copper is then electroplated on top of the gold. Finally, a thin layer of gold is electroplated on top of the copper. The two layers of electroplated gold are each about 3 μ thick, and the copper is 50 μ thick.

B. Windings and Insulation

The multilayer characteristic of a FLO device is illustrated in Figure 9, which shows a cross section of the device at an aperture. Note that one surface of the ferrite (bottom surface in the illustration) does not have a shield on it because this would constitute a shorted turn around a magnetic path. On both the top and bottom surfaces of the

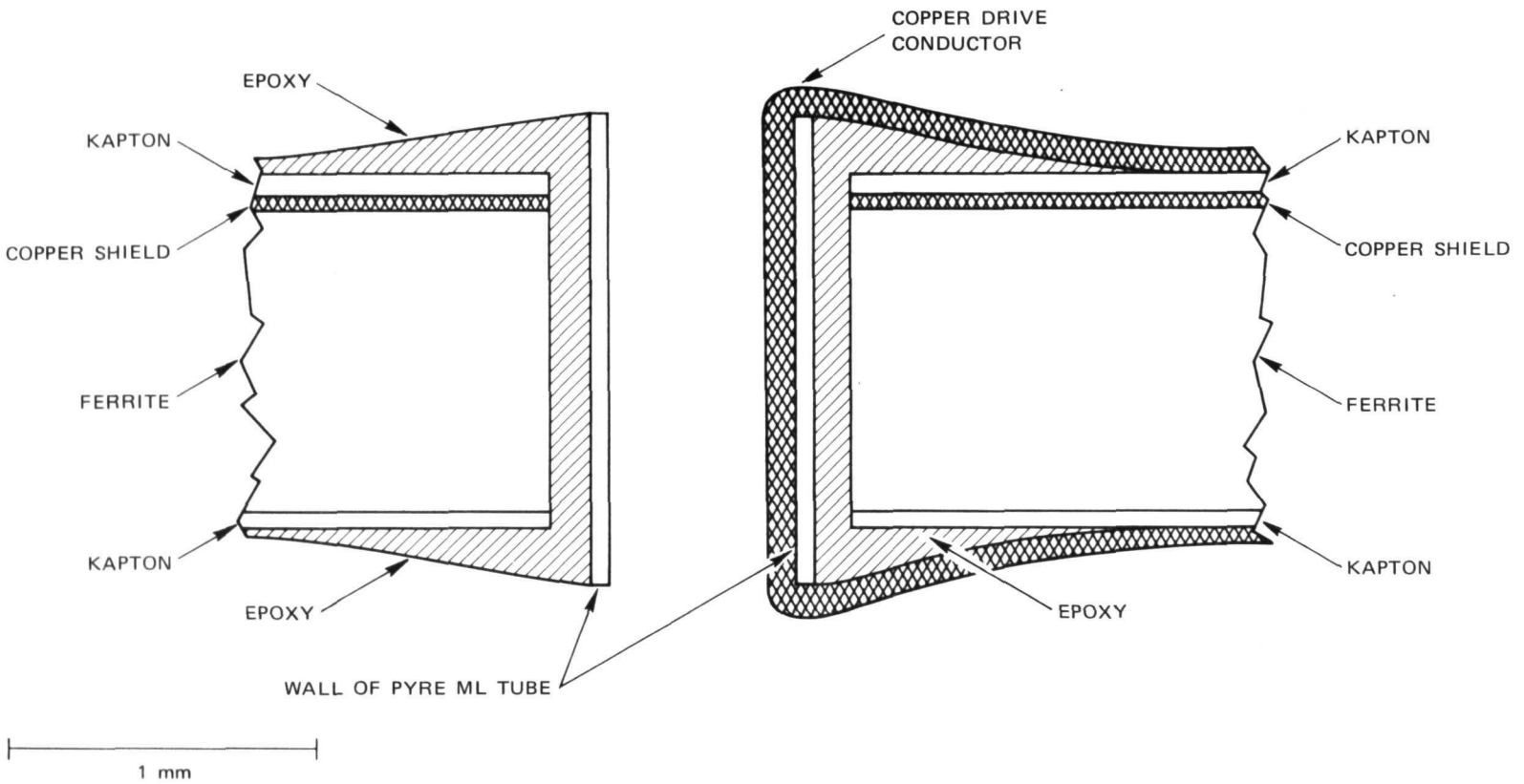

FIGURE 9 CROSS SECTION THROUGH AN APERTURE

shielded ferrite, a Kapton* sheet is bonded with epoxy. The Kapton sheets are 0.05 mm in thickness and both sheets have a conductor pattern on them. The epoxy holding the Kapton is partially cured and then a thin-walled Pyre-M.L.* tube† is inserted into each aperture and at selected places around the periphery of the multipath core. (Kapton and Pyre-M.L. are similar polyimide, thermoplastic, dielectric substances.) Referring to Figure 6, at each numbered location there is a Pyre-M.L. tube except for Location 18.

At this point in the fabrication process, the epoxy is cured. The conductor patterns on the top and bottom Kapton sheets are connected together by "writing" through the Pyre-M.L. tubes and on the epoxy with a special tool similar to a hypodermic needle which deposits liquid gold resinate on the surface. The purpose of this step is to provide a thin metalized base for plating. A three-dimensional wiring pattern is obtained in this manner.

The gold resinate is cured by heating to 300°C. It would be desirable to use a resinate that cures at a lower temperature, but none has been found with the other necessary characteristics. At this point, all the conducting paths necessary for the drive windings have been formed on dielectric surfaces; however, these conductors are not thick enough to provide low resistance paths. The thickness of the conductors is increased by first electroplating gold and then copper on the conductor pattern, as was done for the eddy current shield. The plating builds up conductor thickness inside the Pyre-M.L. tubes as well as on the Kapton

---

*Trademark, DuPont.

†The small insulating tubes are made from commercially available insulated magnet wire. The developers found that after heating a section Pyre-M.L. insulated wire a long thin-walled cylinder of plastic can then be slipped off the magnet wire and cut to the desired length.

and epoxy surfaces. The overlap joint between the gold resinate and the conductor pattern on the Kapton is masked by the copper plating; hence, a conductor path is fabricated without a joint.

It is important to note that at this partially fabricated state the FLO device has been elevated to a temperature of 300°C. In order to fabricate a coupling loop winding (Figure 3), it is necessary to put another layer on top of the multilayer configuration shown in Figure 9. This coupling loop layer comprises Kapton sheets and Pyre-M.L. tubes that are bonded in place with epoxy. A gold resinate coupling loop winding pattern is applied by means of the writing head on the Pyre-M.L., Kapton, and epoxy surfaces. As before, the resinate is cured at 300°C, gold plated, and then plated with copper. Note that this is the second time in the fabrication procedure that the device has been raised to a 300°C temperature.*

Figure 10 shows, at approximately 200 times magnification, a cross section of the interface of the several materials we have been discussing. The several materials can be identified in the photograph as follows: (1) ferrite, (2) copper eddy current shield, (3) epoxy, (4) Pyre-M.L. tube, (5) Kapton sheet, and (6) copper drive conductor. The graduated scale superimposed on the photograph is calibrated at 5.2 μ per small division. The vertical lines in the Pyre-M.L. tube are the boundaries of individual layers of this laminated dielectric. This particular photograph shows Location 74 in cross section. This tube is not within an aperture of the ferrite, hence the copper shield underlays the tube in this area. The layer of gold upon which the copper is plated is not evident in this photograph.

---

*Further details on the production process are given in Reference 3.

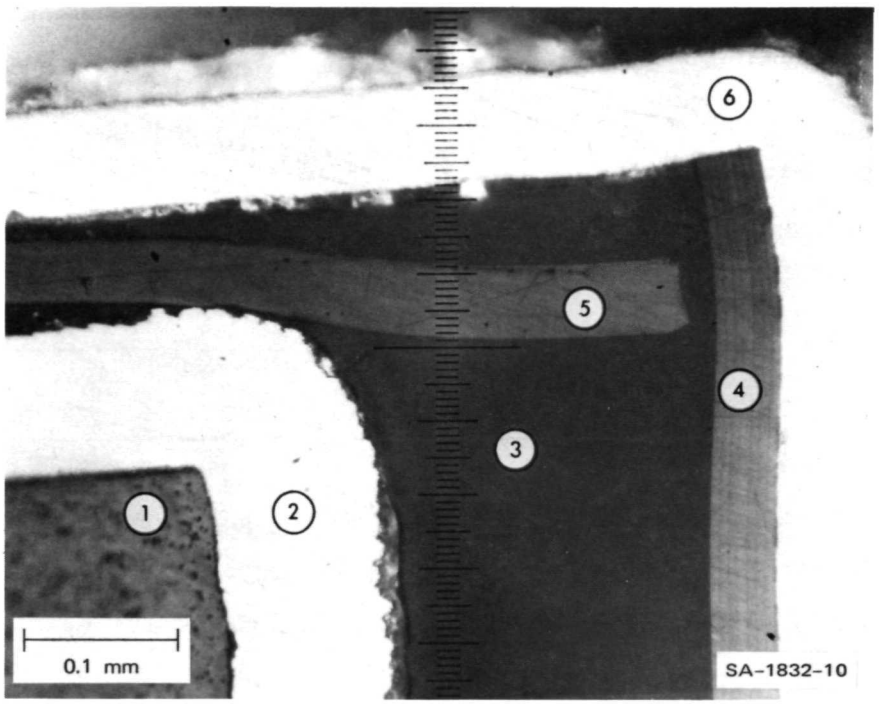

FIGURE 10 MULTILAYER INTERFACE CONSTRUCTION AT 200X

V RELIABILITY OF THE DIELECTRIC/CONDUCTOR SYSTEM

A. Conductor Integrity

In these devices, the conductor pattern overlays the dielectric surfaces of Kapton, Pyre-M.L., and epoxy. The conductor portions that are on Kapton are sometimes given mechanical support by the bond between the Kapton and underlaying ferrite, and sometimes are unsupported. In Figures 6 and 7, the conductor segments that overlay white background regions are unsupported in the sense that the white regions are air pockets (voids) underlaying the Kapton sheet. This gives rise to some concern about the mechanical integrity of these conductors under mechanical and thermally induced stresses that will flex the conductor. Over a protracted period of time, flexing could change the resistance of windings and ultimately lead to open circuits. In addition to unsupported Kapton, another mechanical support problem arises because the conductors sometimes do not adhere to the Kapton. Some means needs to be provided for giving adequate mechanical support to conductors; RTV Silastic* has been suggested. Since the test specimens examined were not in the final package form, some conclusions drawn are, of necessity, tentative. As a part of the final packaging, a means needs to be developed for interconnecting several circuits into a larger system before the conductor/dielectric reliability can be fully assessed.

We have subjected specimens to various environmental stresses in an attempt to accelerate failures. The majority of the observed failures have been of an early-life and quality-control nature rather than related

---

*Trademark, Dow Corning.

to long term catastrophic or degradation failures. Environmental stressing has not induced conductor failures, but we have detected shorts and, in one instance, an open circuit before stressing. These failures relate to control of the fabrication process and are attributed to the lack of process maturity, and the complex nature of the device realization and fabrication processes. Visual inspection of the conductor segments within the Pyre-M.L. tubes is difficult to carry out satisfactorily. Incipient failures could go undetected during the quality control part of the manufacturing process. Electrical measurements alone are not adequate to detect these failures, so quality control of the several windings is difficult.

We have subjected two test specimens to temperature cycling and heat soaking for a five-month period without finding significant changes in conductance. One specimen was subjected to sinusoidal vibration at an acceleration of 20 g rms for more than 700 hours without conductor system failure. Measurements performed on the plated copper indicate that the metal per se has acceptable ductility.

One rationale for the fabrication technique that has been developed for these devices is to obtain a joint-free conductor system. We have found no indications that this goal has not been achieved at the device level; however, the interconnection of several devices into a subsystem in final packaged form has not yet been achieved.

The adhesion between plated conductors and Kapton is a problem not completely solved by the developers. Roughening the Kapton surface by sand blasting has been used to promote adhesion, but we concur with the view of the developers that this procedure is not easily controlled and a better solution should be found. In some instances, we have found pin holes through the Kapton, apparently caused by the sand blasting. Plated copper will deposit in these holes even in the absence of a gold resinate

plating base, thus providing a conducting path through the insulating Kapton layer which, of course, could lead to malfunction.

There is a more subtle problem than the mechanical consequences of poor conductor adhesion. Small spaces between the conductor surface and the dielectric surface can, by capillary action, trap wet chemicals (such as plating solution) in voids during manufacturing, and lead to failure over a protracted operating period through chemical contamination.

B. Chemical Contamination

The deposition of gold and copper by electroplating is used to build up thickness of the conductors that comprise the windings for this device. The conductor lines are approximately 0.25 mm wide, and the conductivity required for operation is achieved by building up the thickness of the conductors to 0.05 mm for drive conductors and 0.1 mm for the coupling loops. Electroplating is a good means for achieving such thicknesses; however, since electroplating is a wet chemical process, proper cleaning of the surfaces is required after each immersion in a plating bath. Electroplating of two gold layers and one layer of copper is required for both the drive conductor and the coupling loops; thus, there are six major plating steps in fabricating these windings. The voids in the FLO device make it difficult to achieve proper cleaning.

We have found evidence of chemical residues in significant amounts from insulation resistance measurements and visual inspection before and after humidity exposure. In FLO devices, the conductor paths are insulated from the eddy current shield on the ferrite by either Kapton, Pyre-M.L., epoxy, or a combination of these. One possible mode of insulation failure is breakdown between two or more conductor segments and one of the shields on the ferrite. A failure of this type could cause one winding to short to another winding or to itself; either of these failures would cause circuit malfunction. The insulation resistance

measured from winding-to-winding or from winding-to-shield varies from specimen to specimen. Values as low as several hundred ohms have been measured in some cases, while other specimens have resistance values which are greater than 10^{11} ohms (measured with 50 V applied).* Calculations indicate that the insulation resistance should be of about 10^{16} ohms. We attribute these variations in insulation resistance to chemical residue. Temperature-cycling of specimens sometimes changes the insulation resistance, as does exposure to humidity. In the case of the humidity, the resistance change appears to be reversible.

In some specimens, under high humidity conditions, we have measured an electromotive force between the drive windings and the eddy current shield. In other words, a wet chemical battery exists that is internal to the test specimens under high humidity conditions. The maximum voltage measured between the windings and the shield is 100 mV (using a 10 MΩ input impedance voltmeter). The significance of the internal EMF is that it provides a mechanism for metal ion transport even in the absence of externally applied circuit voltages. Such metal ion transport could ultimately lead to a short circuit; however, these magnetic circuits operate at very low impedances and, therefore, will malfunction only if the spurious path is a very low resistance. Nevertheless, the existence of such a battery is hazardous in a device designed for extremely long life and high reliability.

On many specimens we have seen evidence of chemical residues. Figure 11 shows a specimen shortly after fabrication and Figure 12 the same specimen approximately one month later. Inspection and comparison of the various conductor segments after aging shows a pronounced discoloration and darkening of many regions throughout the specimen. During the one-month period, the specimen was exposed to temperature cycling;

---

*The maximum resistance value that can be measured at 50 V with the instrument used is 2×10^{11} ohms.

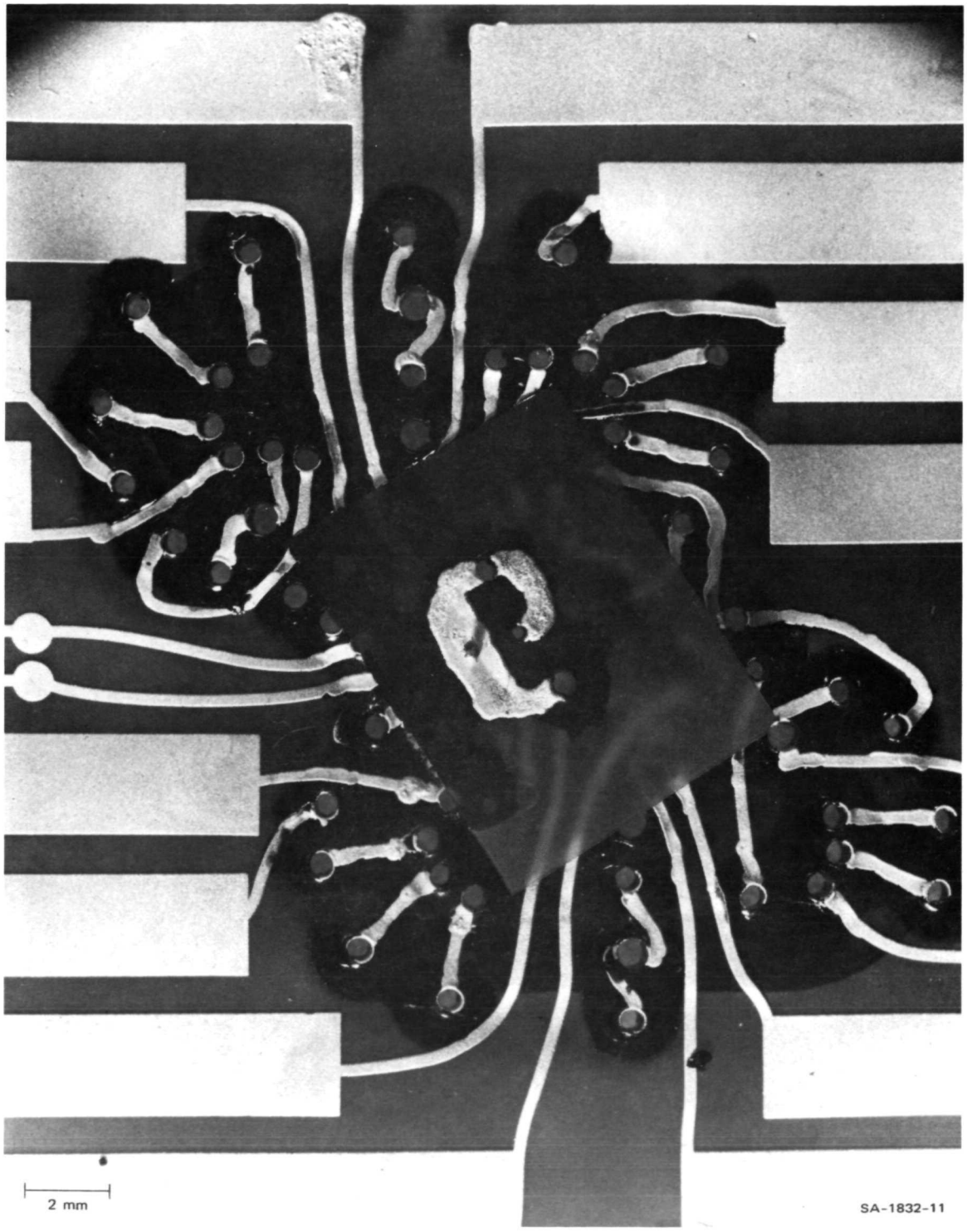

FIGURE 11 TOP VIEW OF NEWLY FABRICATED TEST SPECIMEN

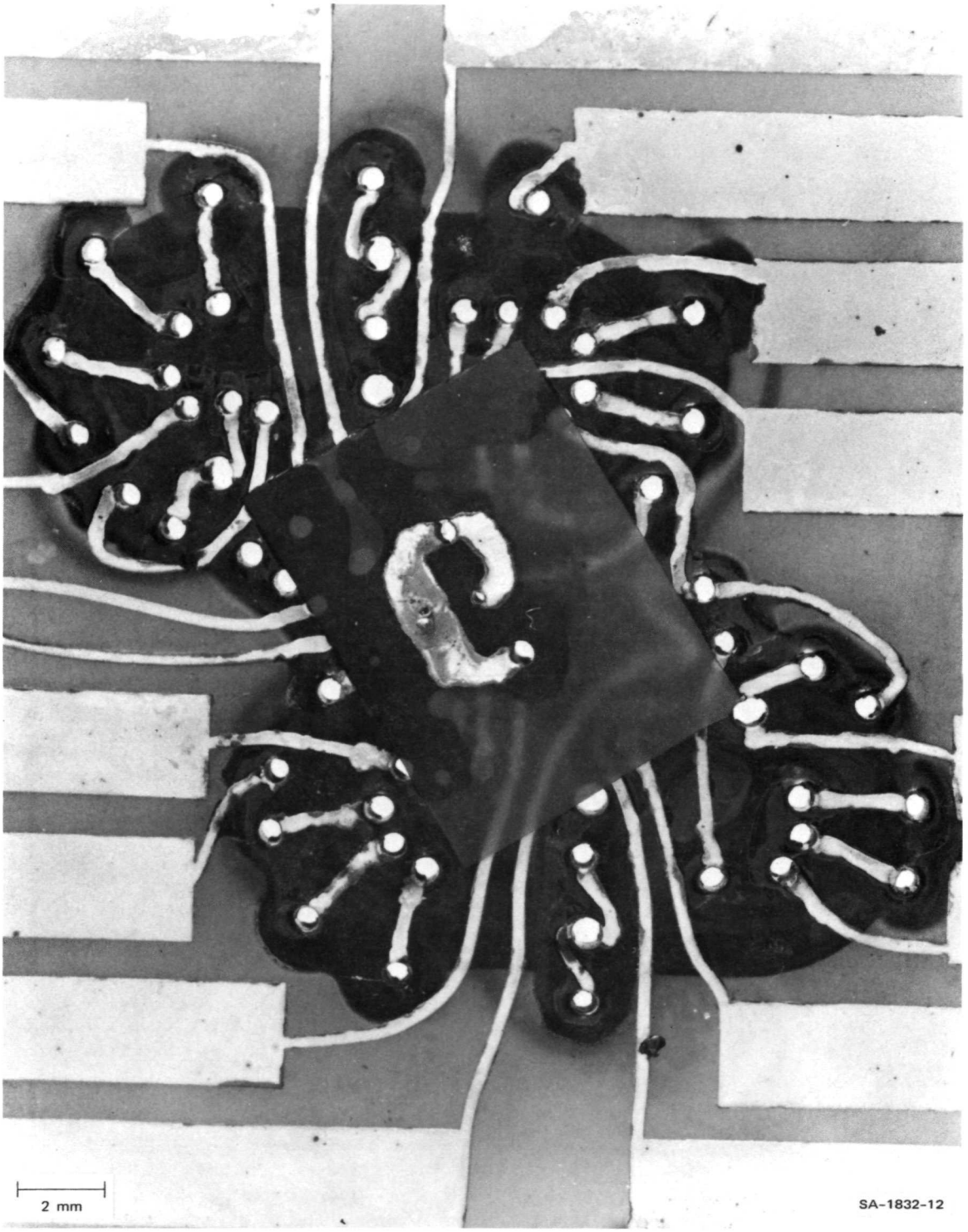

FIGURE 12 TOP VIEW OF SAME SPECIMEN AFTER ONE MONTH

the maximum temperature was + 125°C. Some dark spots on the copper conductor are evident on Figure 11, but most of these spots are epoxy. (One conductor segment that passes between Locations 44 and 45 of Figure 11 shows a dark area that apparently is a shadow caused by the photographic lighting.) Figures 13 and 14 are photographs of the bottom side of the same specimen shown in Figures 11 and 12. Here again, it is evident that the residue is widespread over much of the specimen. The prevalence of the residue along the edges of the segments near the Kapton may mean that it was trapped between the Kapton and the copper conductor. It is important to note that this specimen was exposed only to ambient laboratory humidity.

We have subjected other specimens to high humidity which seemed to accelerate the onset of the visual evidence of the residue. Such exposure also gives a blue-color to the residue, leading us to speculate that part of the residue was hydrated cupric sulphate.

Residue with a somewhat different appearance is pictured in Figure 15. This photograph, taken at 60 times magnification, shows residue that has grown around an unused aperture at Location 57. Residue with this appearance seems to be associated with the copper eddy current shield in our observations. This particular specimen was fabricated without a Pyre-M.L. tube in the aperture, thus enhancing access of the liquid chemicals to the interface between the Kapton sheet and the copper shield. The growth appeared during temperature cycling (up to 125°C) of the specimen over a two-month period.

The fact that chemical contamination remains after fabrication is clearly evident; however, we have not attempted to establish the exact nature of the residue nor its precise long-term effects. The electrical and visual evidence is sufficient to raise serious questions that need to be resolved before high reliability can be assured.

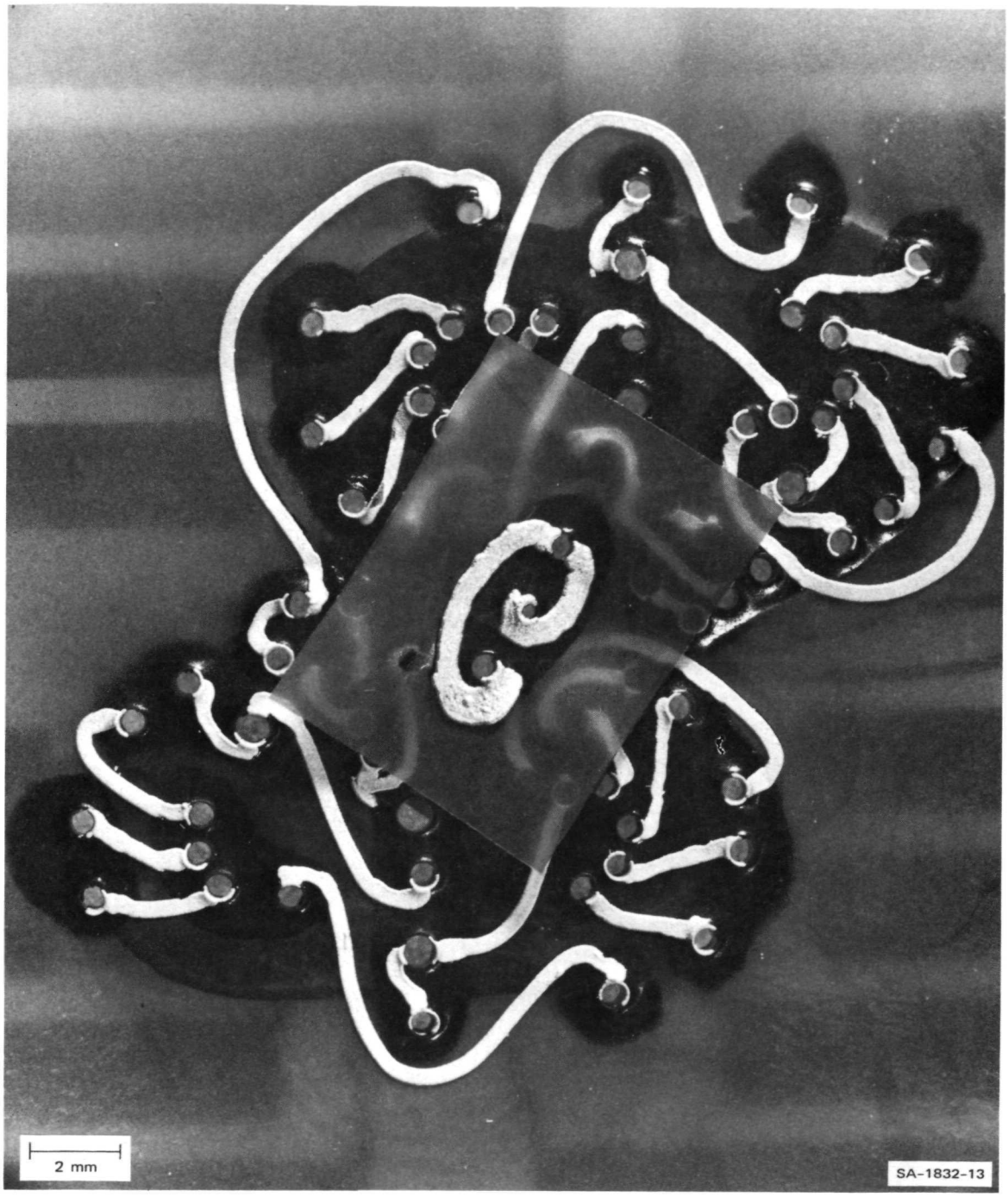

FIGURE 13 BOTTOM VIEW OF NEWLY FABRICATED SPECIMEN

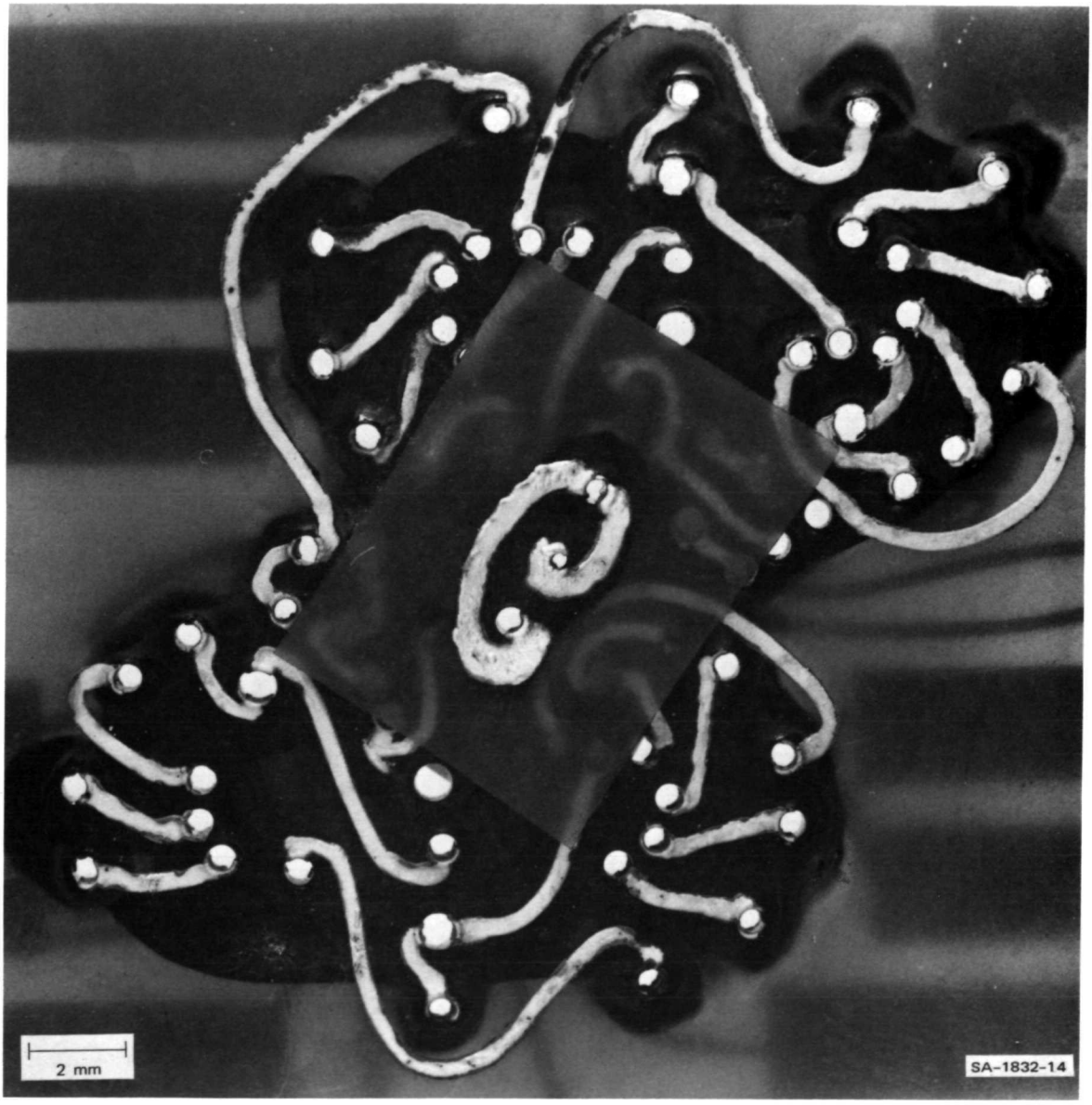

FIGURE 14 BOTTOM VIEW OF SAME SPECIMEN AFTER ONE MONTH

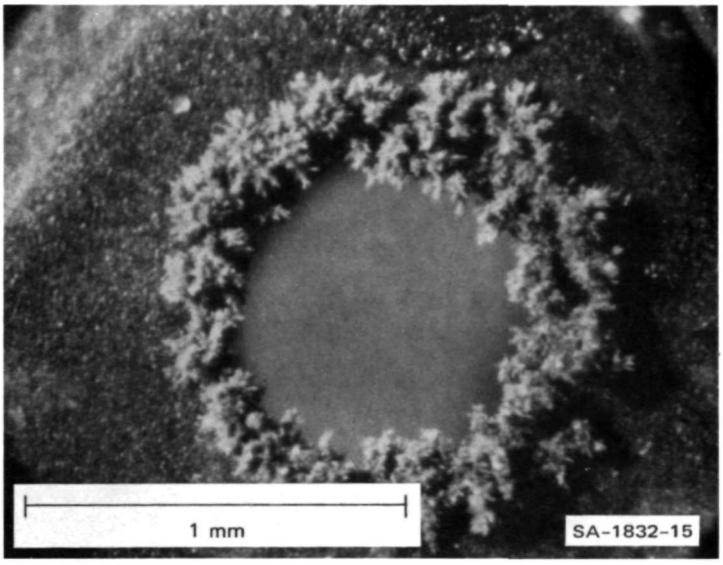

FIGURE 15 RESIDUE AROUND AN UNUSED APERTURE

C. Breaks in the Dielectric Surfaces

Chemical residue can be trapped in cracks and crevices in the Kapton, Pyre-M.L., or epoxy of the FLO device. The geometry of these breaks makes residue removal difficult. In Figure 16, cracks can be seen at the surface of epoxy. Figure 16A shows the bottom view of Locations 68, 69, 71 and 73 at about 30×; Figure B shows the crack between 68 and 69 at about 60×. These cracks (Figure 16A) occurred during fabrication. Figure 17 shows a magnified cross section of the same epoxy crack shown in Figure 16B. (Because of the microscope optics, these pictures are mirror images of the object.) We selected this particular specimen for sectioning because many cracks were visible at the surface. Some other specimens, especially the more recently fabricated ones, do not have many cracks.

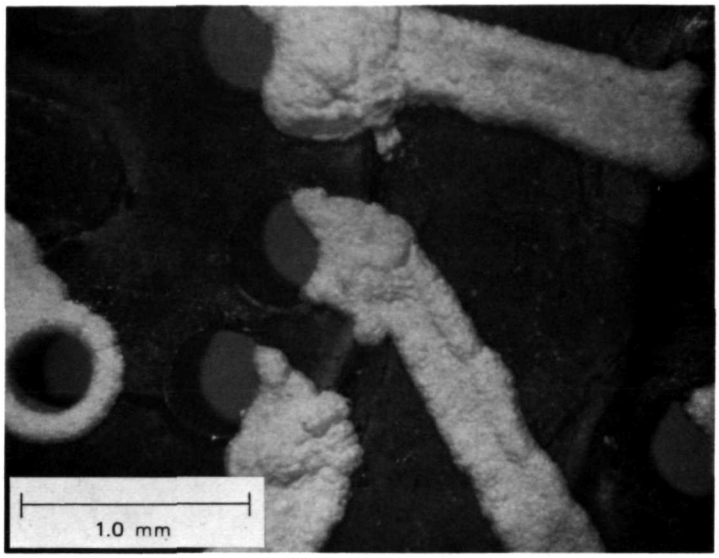

(a) SURFACE VIEW OF LOCATIONS 68, 69, 71, AND 73 AT 30X

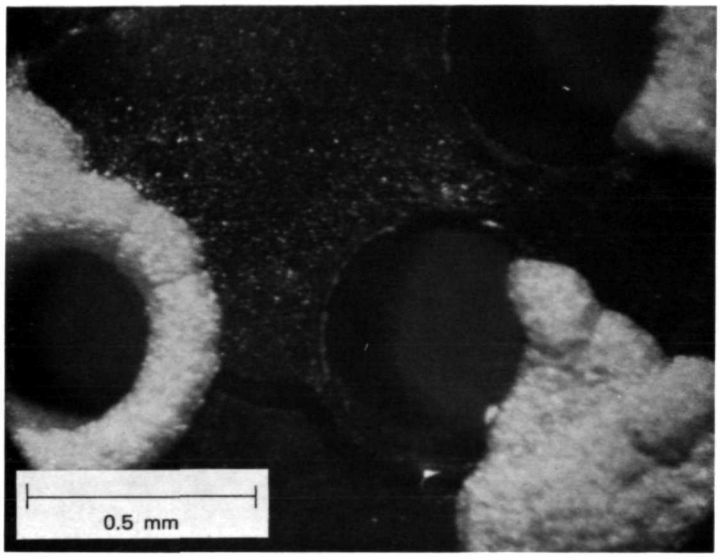

(b) SURFACE VIEW OF CRACK BETWEEN LOCATIONS 68 AND 69 AT 60X

SA-1832-16

FIGURE 16 SURFACE VIEW OF CRACK IN EPOXY

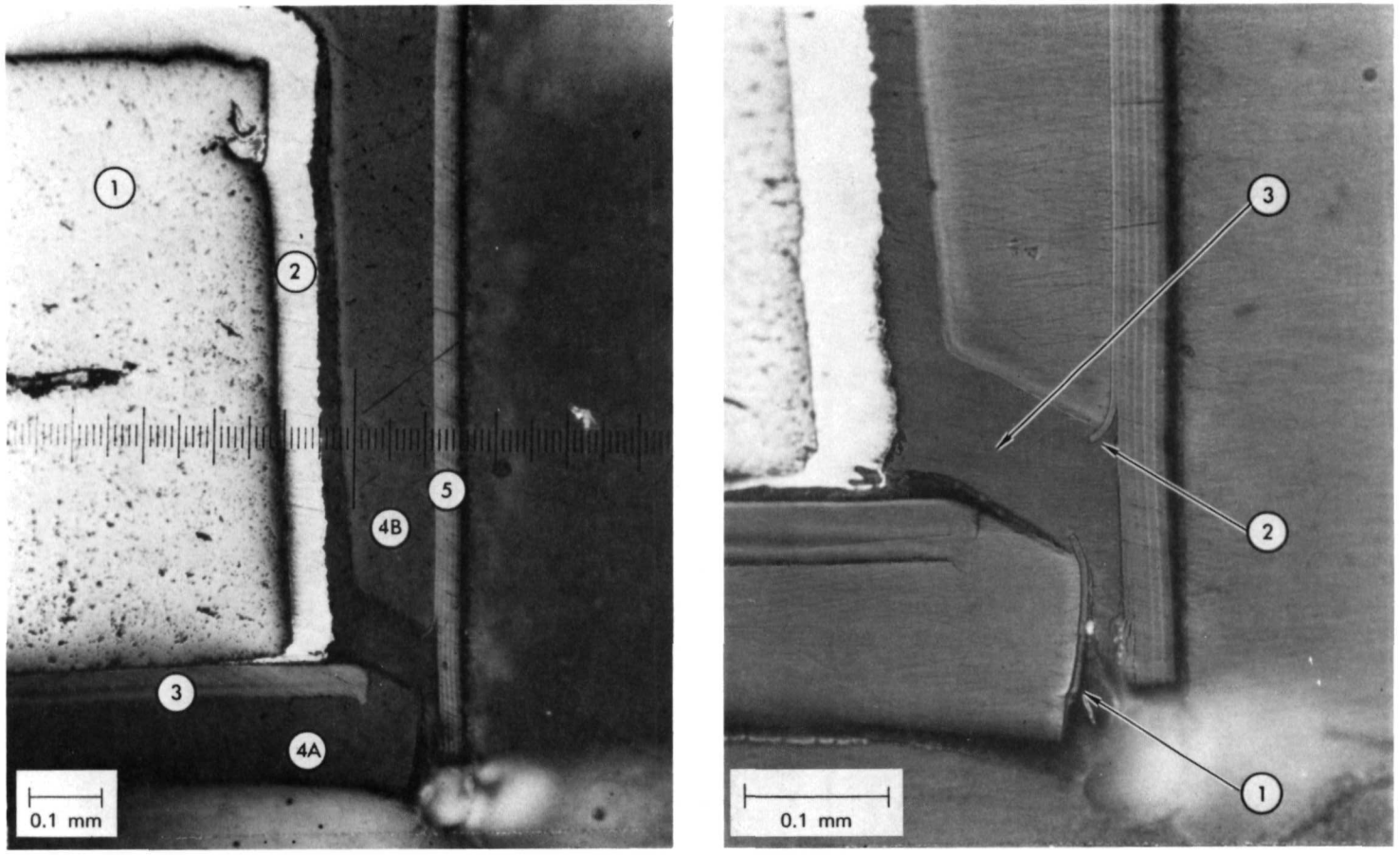

(a) CROSS-SECTION OF CRACK AT 100X

(b) CROSS-SECTION OF CRACK AT 200X

SA-1832-17

FIGURE 17 CROSS-SECTION OF CRACK IN EPOXY

Figure 17A shows the section at about 100 times magnification, and the small divisions on the scale are each equal to 10.3 μ. The region labeled 1 is the ferrite core, and Region 2 is the eddy current shield around the ferrite. Region 3 is the Kapton sheet that is on the bottom of the device. Regions 4A and 4B are epoxy used in the manufacture of the device. The gap between regions 4A and 4B is the crack that communicates with the surface of the device. This crack is filled with casting compound applied under vacuum before sectioning. Note that the crack extends from the bottom surface of the device through a narrow region bounded by the epoxy, 4A, and the Pyre-M.L. tube, item 5; proceeds through the gap between 4A and 4B; and then proceeds along the entire thickness of the ferrite adjacent to the eddy current shield. Figure 17B shows the crack near the surface region at 200 times magnification. Some additional polishing of the specimen was carried out after taking the photograph for Figure 17A and before taking this photograph. Arrows 1 and 2 point to portions of the Pyre-M.L. tube that ruptured when the epoxy cracked. The outside layer of the laminated tube adhered to the epoxy as the epoxy pulled away from the tube. This gives some indication of the strength of the bond between the Pyre-M.L. and the epoxy, and it is important to know that epoxy can induce a rupture in this polyimide. Region 3 is filled with metallurgical casting compound; the light region near the crack at the surface of the device is caused by a bubble in the casting compound.

After additional grinding and polishing, the photograph shown in Figure 18A was taken. This was followed by more grinding and polishing and then the view shown in Figure 18B was photographed. The magnification of both photographs is 100, and the portions of the crack shown are nearer Location 68 than was the view in Figure 16. Note that the character of the crack as shown in Figure 18B is different than it was at the other grinding levels. In Figure 18B the Pyre-M.L. tube is no longer

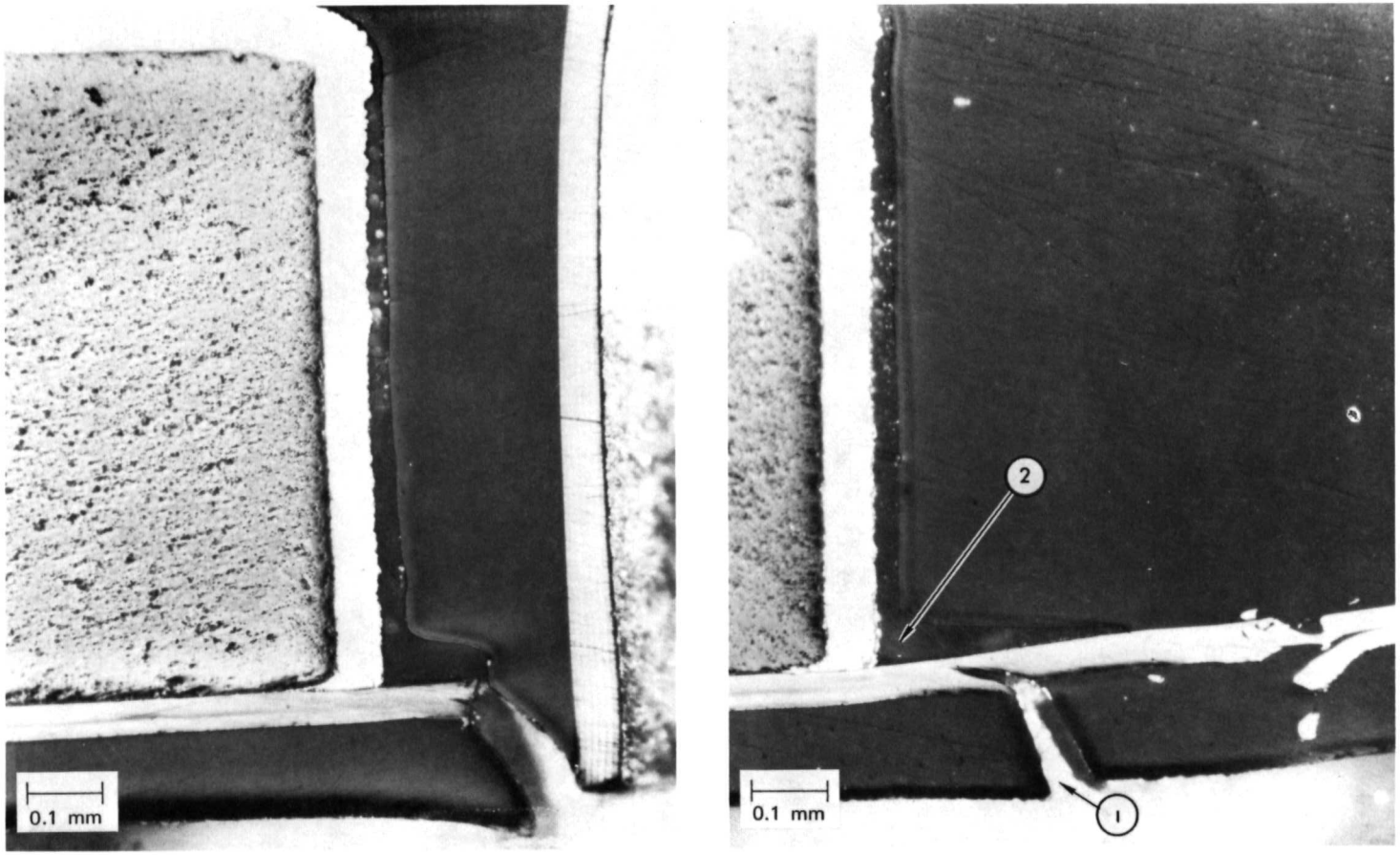

(a) CROSS-SECTION NEAR LOCATION 68 AT 100X

(b) CROSS-SECTION AS IN FIGURE 18A AFTER FURTHER GRINDING AT 100X

SA-1832-18

FIGURE 18 CROSS-SECTION OF FIGURE 16 SPECIMEN AFTER ADDITIONAL GRINDING

visible, the crack no longer skirts the edge of the Kapton, and the Kapton has ruptured part-way through its thickness. Arrow 1 points to the crack at the surface of the epoxy, and Arrow 2 points to the separation of the epoxy from the copper shield. The peculiar jagged rupture of the Kapton shown in the lower right corner of the photograph is of unknown origin.

Figure 19 shows two more instances where the epoxy has caused a rupture in Kapton. Arrow 1 in Figure 19A indicates a region where epoxy is adhering to the Kapton; as the epoxy pulled away by shrinkage, the Kapton ruptured. Region 2 shows Kapton that is not ruptured; epoxy is adhering to only the bottom surface of the Kapton in this region. Region 3 is epoxy that forms the bottom surface of the FLO device. Region 4 is a cross section of a drive conductor attached to the surface of the epoxy and Arrow 5 points to Location 60. Figure 19B shows ruptured Kapton at a magnification of 500 times. Region 1 is epoxy at the bottom surface of the specimen. Regions 2A and 2B were originally one Kapton sheet (the Kapton is approximately 0.05 mm thick). It appears that the Kapton ruptured when the epoxy curled during curing or later.

Figure 20 shows a different type of break in the dielectric surface. Both of these photos show (in mirror image) Location 52, the clipper core, between the Odd and Even stages. Figure 20A, at 200 times magnification, shows a crevice that communicates with the surface as indicated by the arrow. This crevice, which was visible at the surface before the specimen was sectioned, is in fact a separation between two concentric Pyre-M.L. tubes. The outside Pyre-M.L. tube is used as a spacer, as can be seen by looking at Figure 20B (at 63 times magnification). This crevice penetrates approximately halfway through the test specimen. This spacer could be eliminated by redesign of the components, thereby eliminating a residue trap. (The bright horizontal line in the left-hand

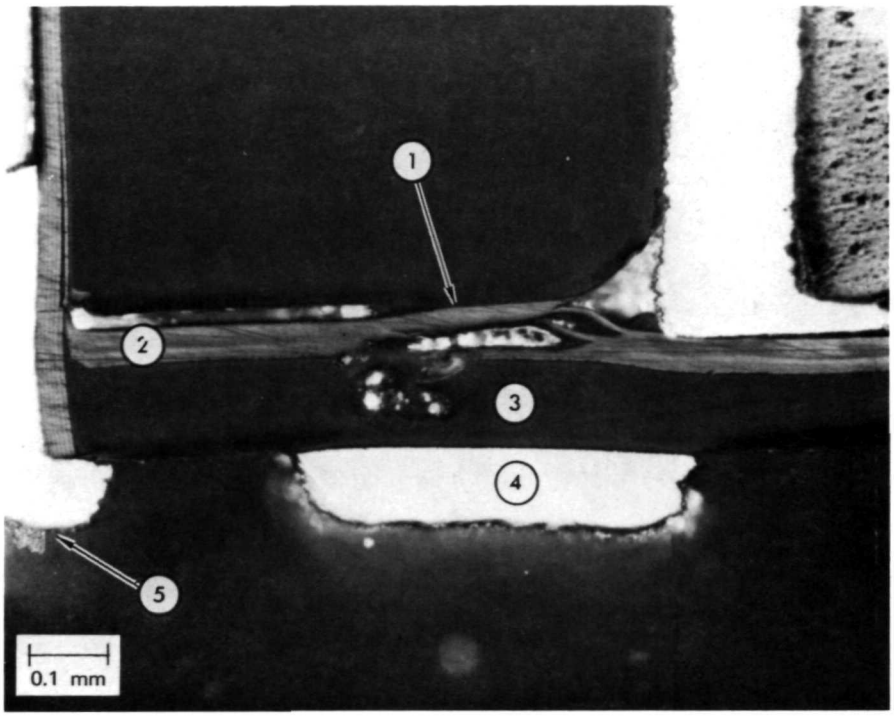

(a) KAPTON RUPTURE AT 100X

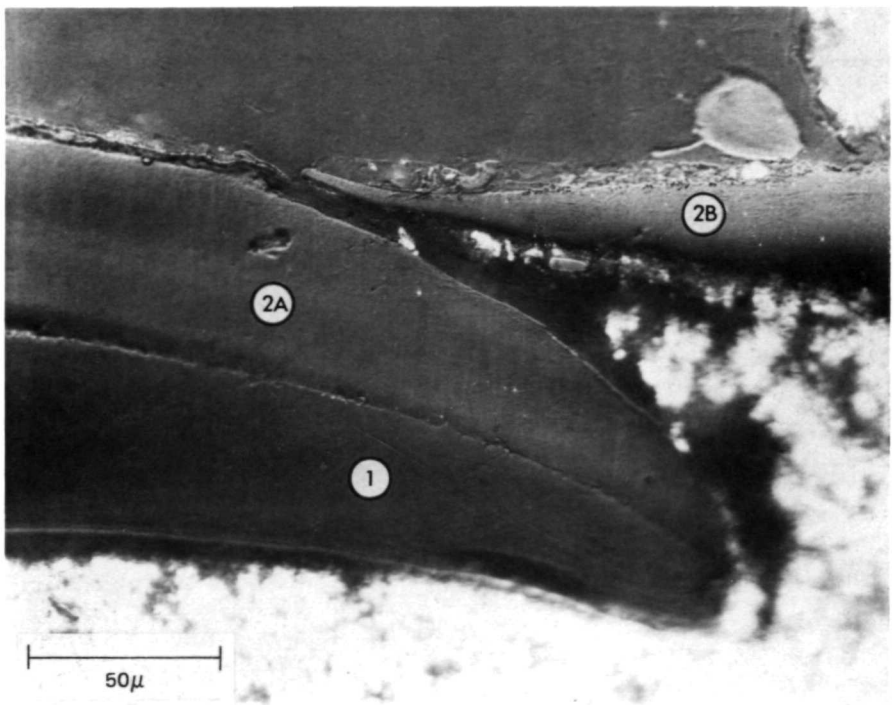

(b) KAPTON RUPTURE AT 500X

SA-1832-19

FIGURE 19 EXAMPLES OF KAPTON RUPTURE

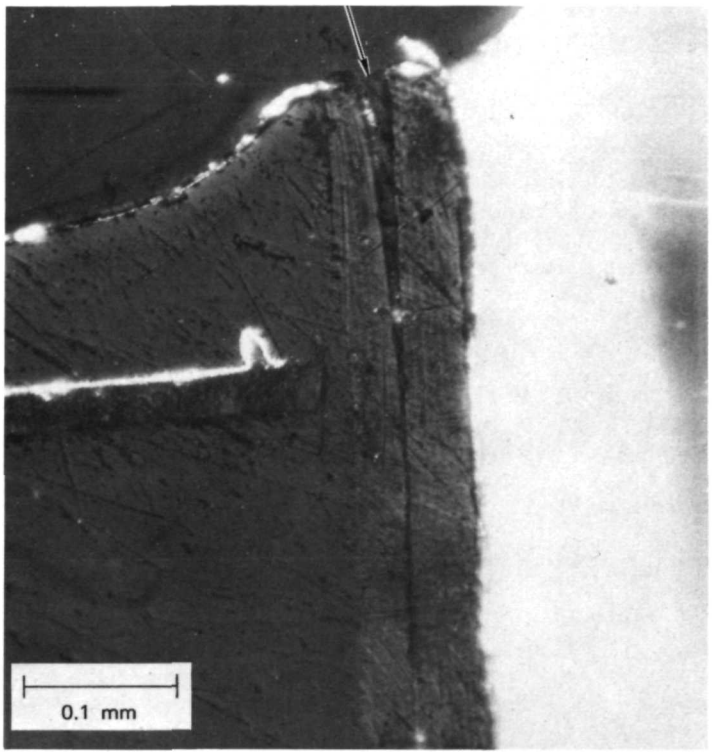

(a) CREVICE TO SURFACE AT 200X

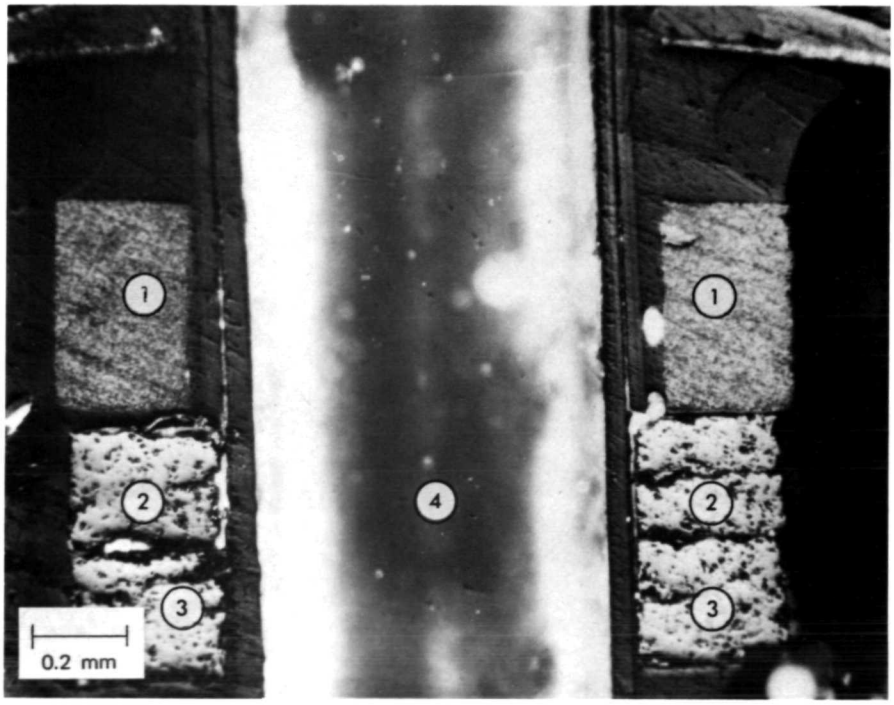

(b) CONCENTRIC TUBES AT 63X

SA-1832-20

FIGURE 20 SURFACE CRACK FROM CONCENTRIC TUBES

portion of Figure 20A is an unused metalized segment on the Kapton surface.) In Figure 20B, Region 1 is the cross section of a nonmagnetic ferrite toroid that functions as a mechanical spacer. Regions 2 and 3 together are a pair of toroids that are used in circuit operation as a single clipper core. Region 4 is filled with casting compound and is the aperture through the toroids.

The laminated construction of the Pyre-M.L. tubes was mentioned in the discussion on Figure 17B, and two concentric tubes are shown in Figure 20. In the next figure, Figure 21, delamination of a tube at the surface of the FLO device is shown at 200×. This delamination could also be seen to some extent by examining the end of the tube. A crack (or

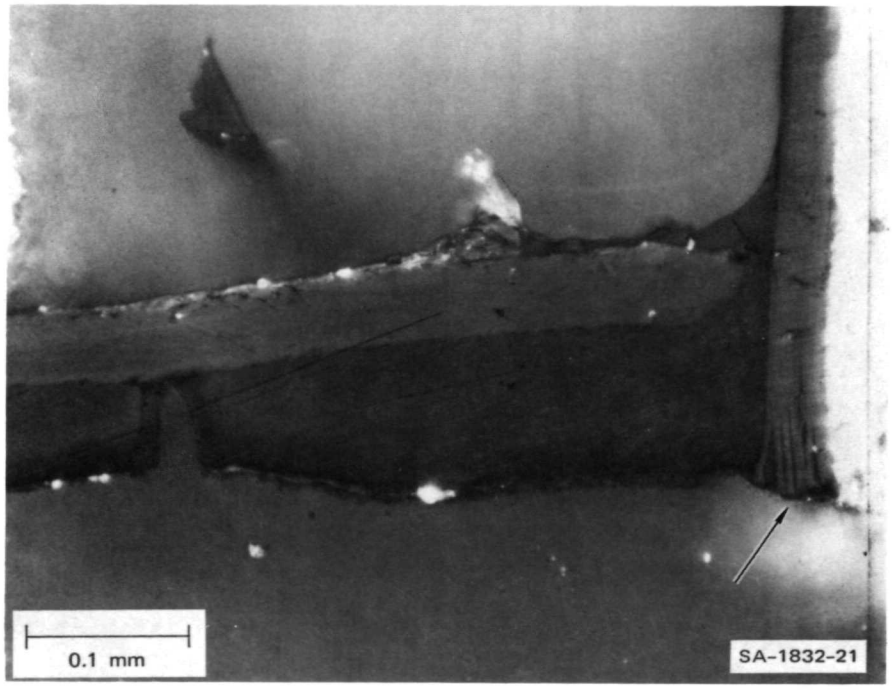

FIGURE 21 PYRE-M.L. TUBE DELAMINATION AT 200X

bubble) in the epoxy that did not propagate into the Kapton is also evident in the photograph.

The breaks in the dielectric surface that occur during the manufacture, in addition to being residue traps, can result in shorts between conductors. Under the best circumstances, this would result in a low manufacturing yield. A more serious problem arises because incipient failure by shorting could go undetected in the quality control procedures and therefore result in failure under operating conditions. Figure 22 shows a short between a drive winding conductor and an eddy current shield through a rupture in the Kapton. This Kapton rupture and the short were created during fabrication. In Figure 22A, Region 1 is the drive conductor and an arrow points to the Kapton rupture and short. Region 2 is epoxy at the surface of the FLO device; 3A and 3B are Kapton, and Region 4 is eddy current shield. The buildup of the gold and/or copper on the surface of the eddy current shield can be seen in Figure 22A. Region 5 is the ferrite. Figure 22A is taken at 100 times magnification and Figure 22B at 200 times. This break occurred at Location 7 on the bottom side of a specimen.

All of the conditions illustrated in Figures 16 through 22 occurred during the fabrication of test specimens; none were induced by environmental stressing. However, we have induced cracks in the epoxy and separations of Pyre-M.L. tubes from the epoxy by temperature cycling specimens from room temperature to +125°C. Chemical contamination and conductor shorts would not result from cracks induced during service; however, these induced cracks do indicate unrelieved stresses that could have long-term reliability implications. A crack in epoxy near or underneath a conductor segment could form a stress concentration that would cause the conductor to open circuit under the influence of thermally induced and mechanically induced strain, repeated often over a prolonged period of time.

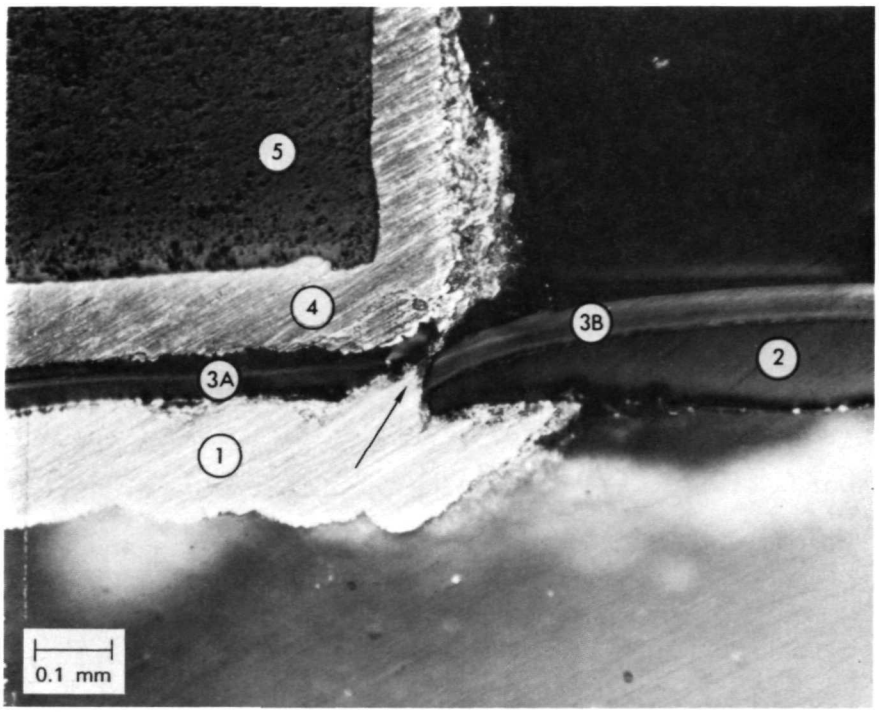

(a) KAPTON RUPTURE AREA AT 100X

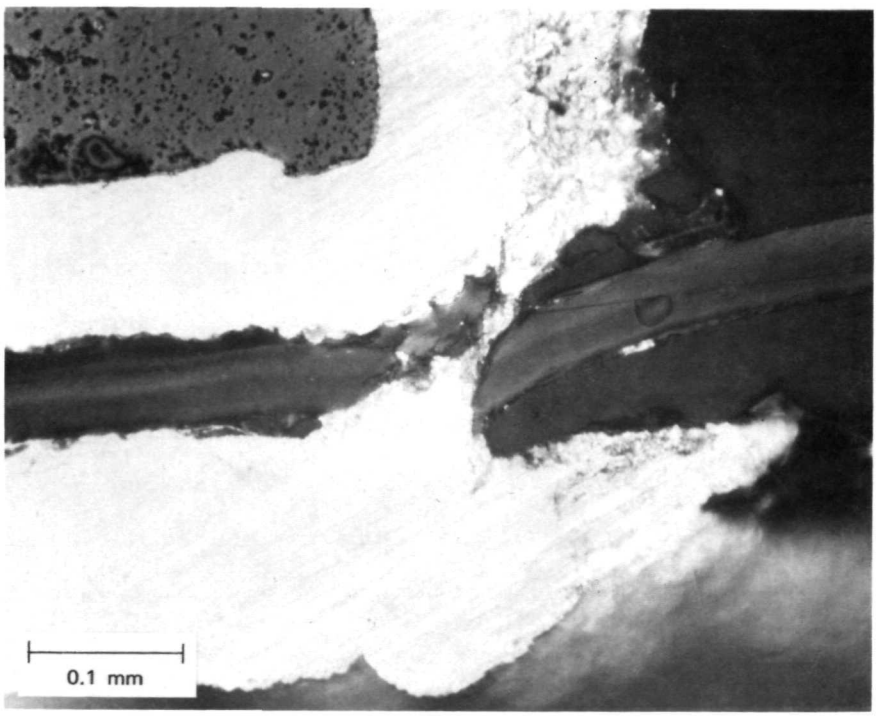

(b) KAPTON RUPTURE SITE AT 200X

SA-1832-22

FIGURE 22 SHORT THROUGH RUPTURE IN KAPTON

The breaks in the dielectric surfaces of the FLO device should be eliminated because of the problems associated with chemical residue, conductor shorts, and conductor open circuits. High reliability cannot be assured until the dielectric imperfections have been eliminated. There are probably two reasons for these breaks in the surface. The nature of the device brings into intimate contact several materials with different coefficients of thermal expansion and therefore one member could induce a strain that exceeds the elastic limit of an adjoining member. In principle, this problem can be eliminated by selecting materials with similar temperature coefficients; however, in practice, this ideal is sometimes difficult to achieve. Limiting the range of temperatures to which the device is exposed can also help solve such a problem, but the developers have failed to find a usable material that cures at a temperature below 300°C. The serious reliability implications of the breaks in the dielectric surface mean that further development work is required before high reliability can be assured.

D. Alternate Coating Approach

In an earlier realization of FLO devices, a conformal dielectric coating was used over multipath ferrite structures. This was abandoned because, among other problems, the coating was thinner at the corners than elsewhere. We have examined the cross section of a ferrite toroid coated by Union Carbide Corporation with their Parylene dielectric. As can be seen in Figure 23, the Parylene conforms well to the contour of the ferrite at the corners and on the planar surfaces. The magnification for Figure 23A is 75×; for Figure 23B the magnification is about 500× with the small-scale divisions each equal to 2.2 μ. If the use of a conformal coating is reconsidered, the Parylene process should be investigated for its suitability to this application.

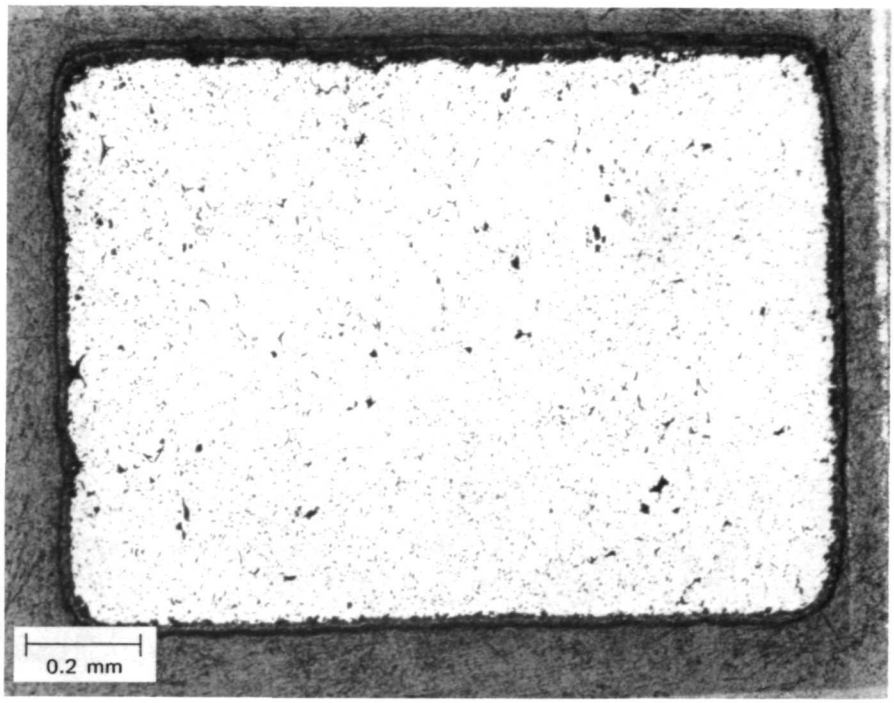

(a) PARYLENE DIELECTRIC COATING AT 75X

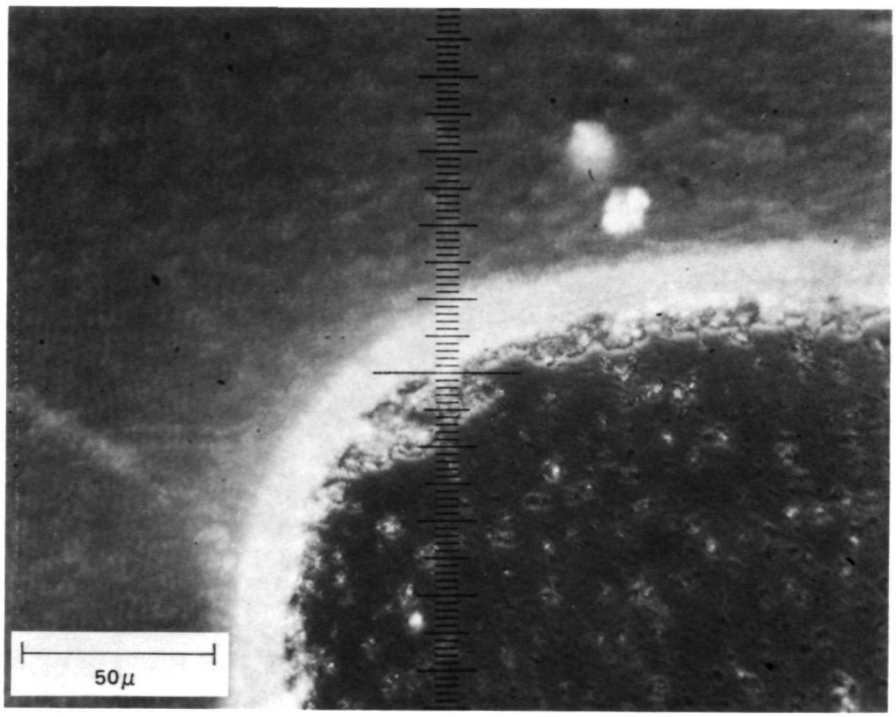

(b) PARYLENE DIELECTRIC COATING AT 500X

SA-1832-23

FIGURE 23 CROSS-SECTION OF ALTERNATE COATING APPROACH

VI RELIABILITY OF THE MULTIPATH MAGNETIC FERRITE

A. High Coercive Force Regions

Failure by degradation of magnetic characteristics in the multipath ferrite can arise from two sources: magnetostrictive effects that arise from mechanical stress applied to the ceramic material, and cracks in the ceramic that appear magnetically as an air gap. The magnetostrictive related effects are reversible and the original characteristics are recovered when the applied stress is removed. We have found no evidence of failure due to magnetostriction; if it is a problem, it has been masked by other effects. The cracks in the ferrite ceramic are not reversible and cause permanent degradation of performance and/or catastrophic failures. Degradation would first become evident at the extremes of temperature operating range and at the extremes of the drive (clock) current pulse-amplitudes. As the crack size increases, operating margins would decrease accordingly.

The bimaterial nature of the FLO device is an important operational feature. The interface of the two ferrite compositions is a logical place to expect cracks to develop in the ceramic. In some specimens we have detected cracks in the ferrite in both the high coercive force material and the low coercive force material, but none of the specimens have displayed cracks at the interface of the two materials, as determined by both magnetic measurements and visual observation of polished specimens. An example of the effect a crack (or cracks) has upon the magnetic φ-F characteristics is shown in Figure 2. The several figures discussed below show the details of some cracks that we have detected and studied visually under a microscope.

Figure 24 shows a crack through the thickness of the ferrite near Location 71. Figure 24A has magnification of 65 and Figure 24B a magnification of 200. Evident in Figure 24A are breaks in the epoxy bond between the copper eddy current shield and the epoxy, and between the epoxy and Kapton in the lower part of the picture. A small crack in the Kapton can be seen at the top of Figure 24A, and at the bottom there is a rupture that goes completely through the Kapton. (This same Kapton rupture was shown in Figure 19B at a greater magnification but at a different grinding depth.) Figure 25 shows at 100 times magnification the same crack pictured in Figure 24 after additional polishing to reveal changes in the nature of the crack as a function of depth into the ferrite.

Another crack, shown in Figure 26 at 100 times magnification, is near a drive aperture, Location 65. Note that this crack has the same character as the previous one in that it proceeds completely through the thickness of the ferrite from one end to the other, and it is approximately orthogonal to the top and bottom surfaces of the ferrite.

Figure 27 shows a crack near an input aperture, Location 62. The magnification for Figure 27A is 100 and for Figure 27B, which is of the same region, the magnification is 500. In Figure 27A, note the character of the crack about midway through the thickness of the ferrite. A small ferrite "bridge" connects the two main bodies of the ferrite together. This type of crack would not be expected in a brittle material, suggesting that it occurred while the ferrite was still semiplastic, a conclusion supported by Figure 27B. Examination of the interface between the copper shield and the ferrite at this magnification shows intimate contact between the two materials and indicates that the crack existed before the metal was deposited on the ferrite surface. There is no indication of slippage between the metal and ceramic, or of a stretching of the ductile metal during the creation of the crack. The characteristics of the crack shown in these two photographs suggest that it

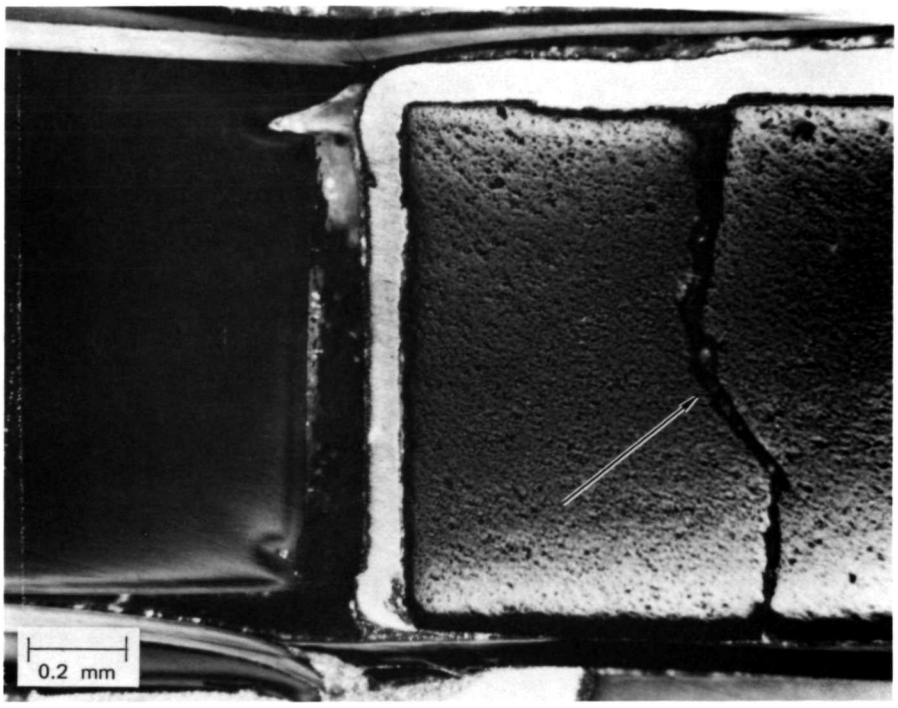

(a) CRACK IN RETURN LEG AT 65X

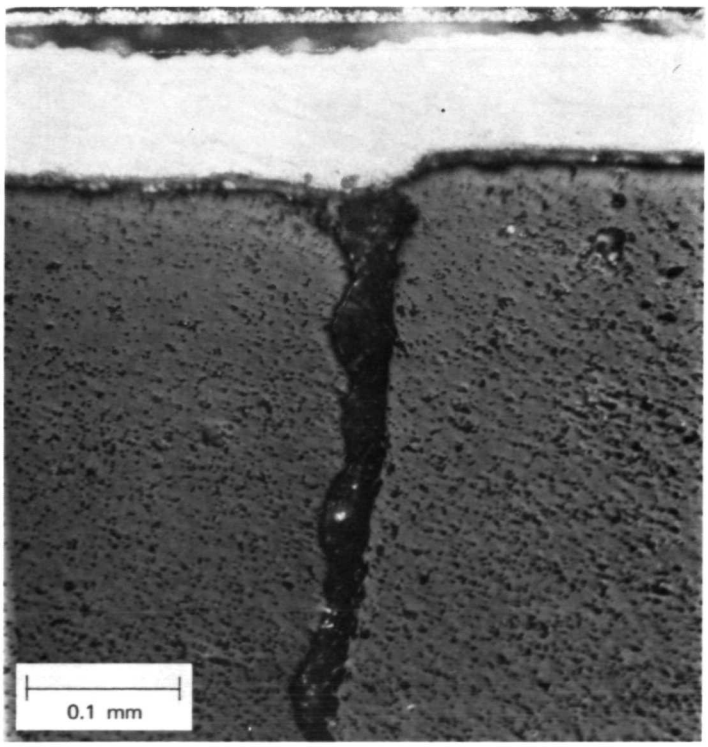

(b) CRACK IN RETURN LEG AT 200X

SA-1832-24

FIGURE 24 CRACK IN RETURN LEG

FIGURE 25 CRACK IN FIGURE 24 SPECIMEN AFTER GRINDING AT 100X

occurred in either the compression-bonding stage of the fabrication or during the firing of the ceramic, the latter being more probable.

B. Low Coercive Force Regions

All of the cracks discussed above occurred in the high coercive force ferrite composition. Figure 28 shows a crack in the low coercive force composition surrounding the output aperture. (The magnification for this photograph is 100 times.) The low coercive force composition has a finer textured appearance and is on the right in the figure. The high coercive force composition on the left-hand side has more small voids in it. Two regions at the interface in the center of the photograph have the appearance of large voids. These may be associated with the bimaterial interface,

FIGURE 26 CRACK NEAR DRIVE APERTURE AT 100X

but this is the only indication we have seen of a discontinuity at the interface. The position of the crack in the low coercive force composition is probably related to a corner in the geometry of the device, and hence a stress concentration point, rather than related to the bimaterial composition.

The cracks shown in Figure 29 are in a specimen rejected by the developers during quality control after device fabrication. These photographs were taken at a magnification of 32 times. Figure 29B shows the output aperture at Location 21, and Figure 29A the output aperture at Location 54. The bimaterial feature is evident in both of these photographs. The cracks in both of these photographs do not show any relationship to the interface of the two materials. There are cracks

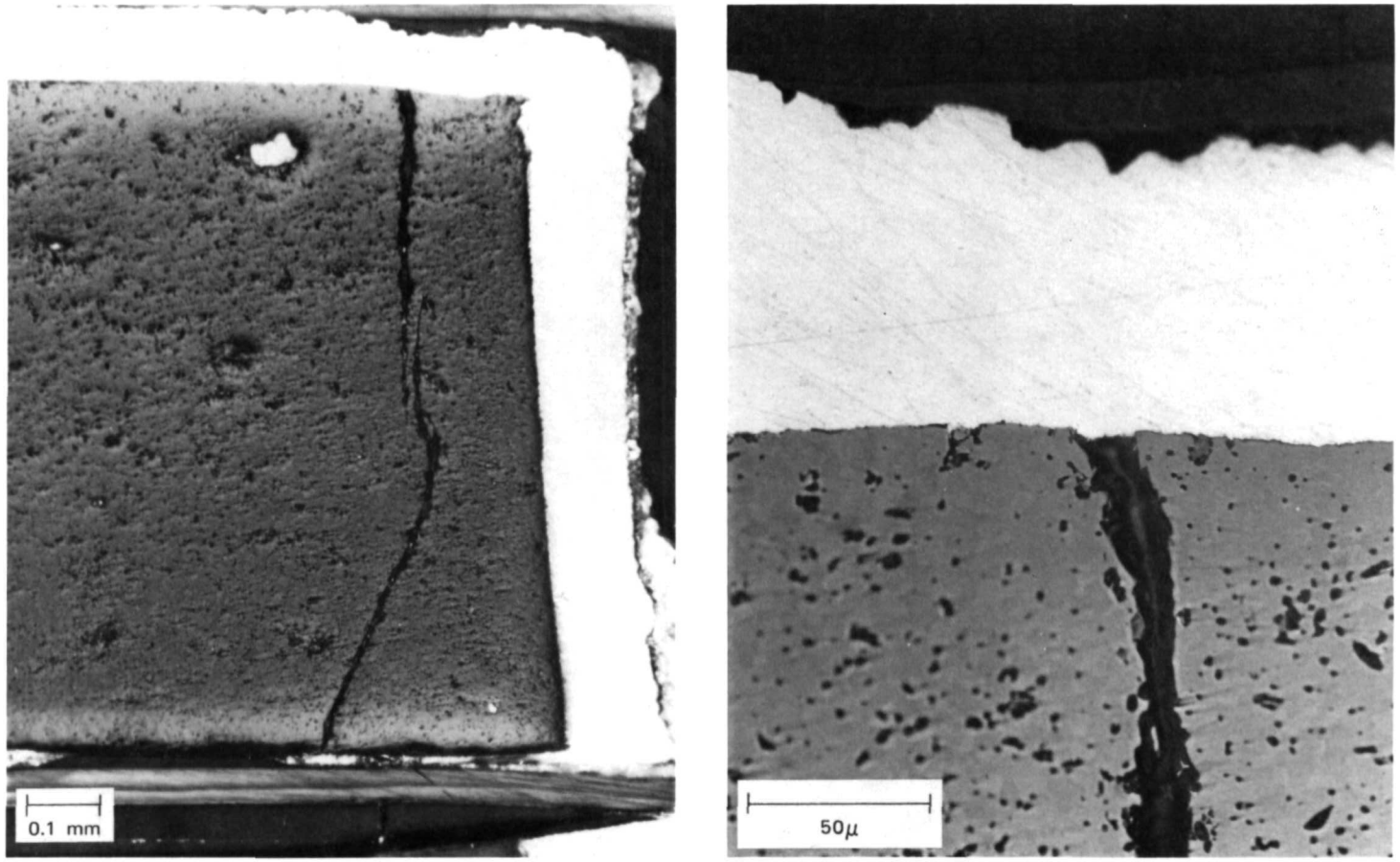

(a) INPUT APERTURE CRACK AT 100X

(b) SHIELD AND CRACKED FERRITE INTERFACE AT 500X

SA-1832-27

FIGURE 27 CRACK NEAR INPUT APERTURE

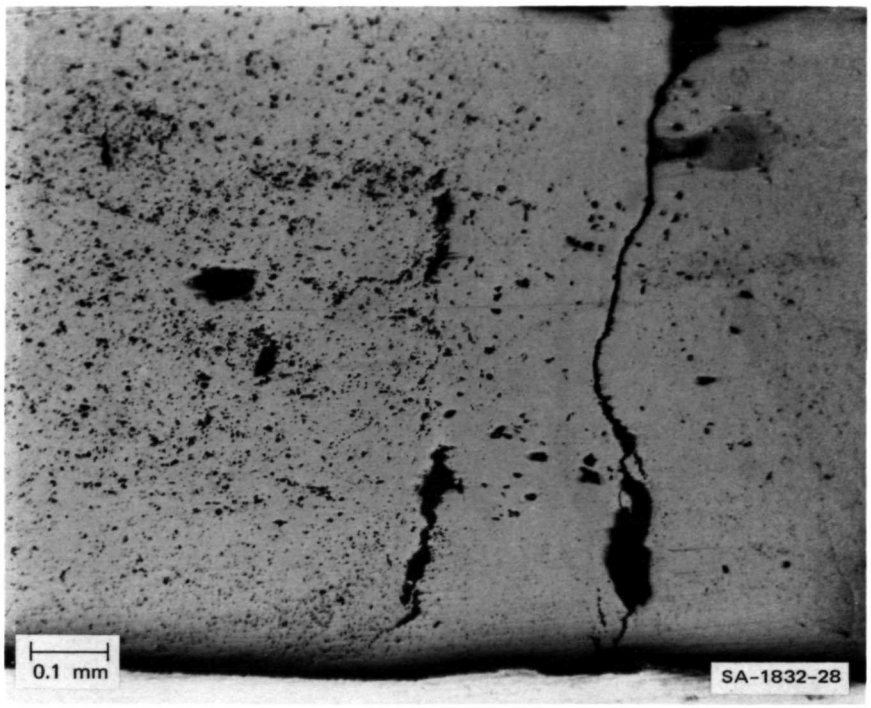

FIGURE 28 CRACK IN LOW COERCIVE FORCE COMPOSITION AT 100X

in both the high and low coercive force compositions. The position and direction of the cracks appear to indicate geometric origins. In Figure 29A, two drive winding segments and two coupling loop segments are visible in the aperture. In Figure 29B, two drive winding conductor segments are visible in the aperture. The white circular regions on the periphery of the photograph are conductor segments going through Pyre-M.L. tubes that do not lie within an aperture.

C. Consequences of Cracks in Ferrite

We have carried out some limited experiments in an attempt to induce crack growth in specimens known from magnetic measurements to be cracked, and also in specimens having no cracks indicated by magnetic measurements.

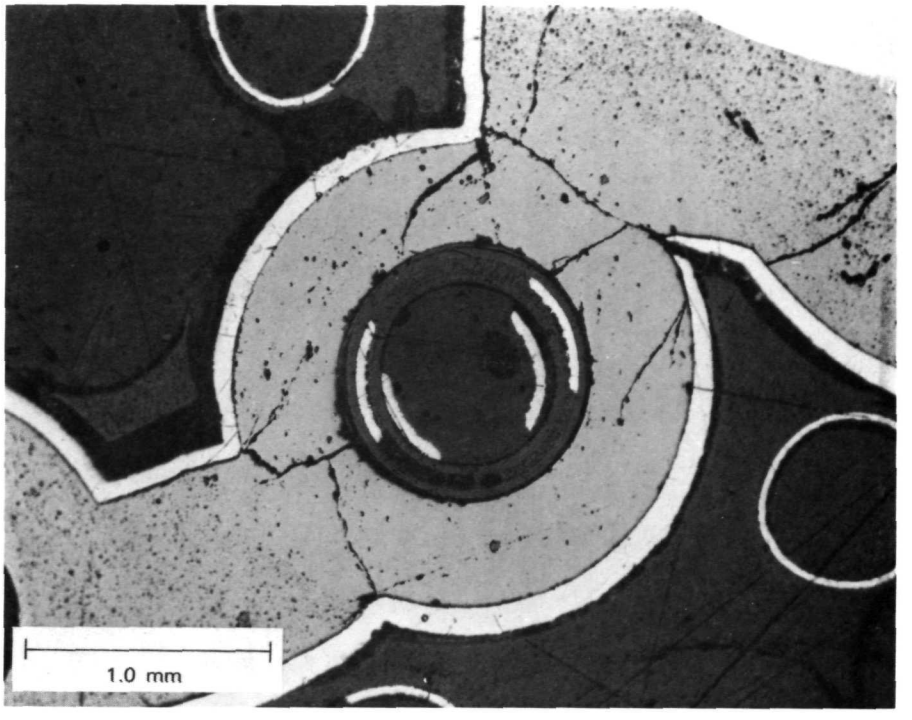

(a) CRACKS NEAR LOCATION 21

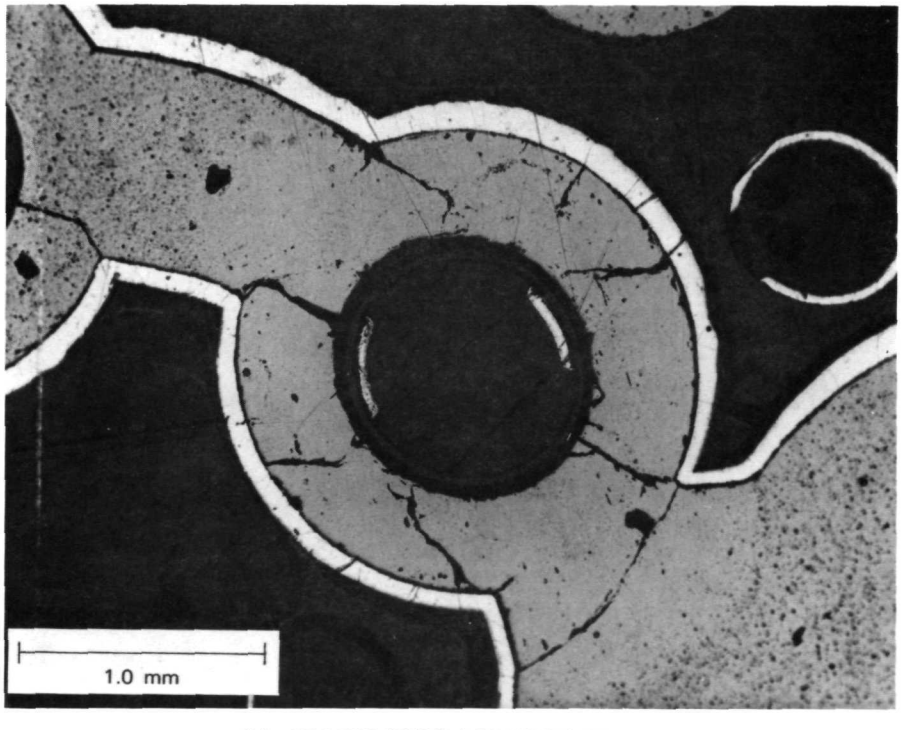

(b) CRACKS NEAR LOCATION 54

SA-1832-29

FIGURE 29 CRACKS IN A REJECTED SPECIMEN AT 32X

Specimens were subjected to temperature cycling from +25° to +150°C and sinusoidally vibrated at 20 g rms. No changes were observed in the magnetic characteristics. This may indicate that the internal stresses were relieved in the fabrication process, or that a more severe environmental condition is required in order to induce crack growth.

The cracks that occurred during fabrication as illustrated in the figures are not at an acceptable level for a high quality device. In addition to any long-term effects that might result from these cracks, it is probable that the observed variations in magnetic characteristics from specimen to specimen can be attributed, in part, to the existence of these ferrite cracks. We have observed significant specimen-to-specimen variations in the flux gain characteristic, in the static φ-F characteristic, in the value of the remanent flux around output apertures, and in optimum amplitude values for the pulse drive current. Cracks in the ferrite could contribute to, or be totally responsible for, all of these variations.

Improved ferrite processing techniques should eliminate these cracks. Since the cracks are not related to the bimaterial feature of the FLO device, high-quality control precautions should prove adequate. However, magnetic measurements alone are sometimes inadequate for detecting the cracks. To illustrate this point, on one specimen that passed the developers' quality control procedures and was accepted as being a good core, our magnetic measurements similarly revealed no anomalies; however, subsequent microscopic examination revealed cracks in the high coercive force material. This seems to indicate that improved quality control techniques need to be developed and applied routinely in the fabrication procedure.

VII RELIABILITY PREDICTION

A. Materials, Processes, Devices, and Systems

Either catastrophic or degradation failures can cause a system to fail, but the entire system must be considered before making a reliability prediction for all modes of failure. In some systems there is little interaction between devices, but in FLO systems, the relationships are more intimate, since drive windings are coupled in series to all of the devices. The first order of faults occur at the device level, but reliability prediction is made at the system level. In the present study, the greatest emphasis has been directed toward materials and devices, because the failure modes of elements and of devices must be understood before system reliability predictions can be made. The following discussion considers failure modes of the elements that comprise devices and systems.

A FLO system consists of a number of FLO devices and appropriate clock generators. The devices consist of complex ferrite structures, insulation, and plated electrical conductors. Failures can occur in any of these elements, and indeed the testing during this project has demonstrated failures within the ferrite structure as well as in the conductors and dielectric. The observed catastrophic failures are numerous, and additional development will be required to reduce this class of failures. Further it seems that the device failure modes are, to a first approximation, independent. For example, the cracks observed in the ferrite structures would cause a device to be inoperative, but there is little reason to believe that the cracks were induced by the subsequent processing that added the dielectric layers and plated conductors.

Similarly, the open circuits in conductors are usually not associated with a failure in the dielectric or ferrite. Improvements will have to be made in the ferrite, in the dielectric, and in the conductors to reduce the catastrophic failure rate to an acceptable level before further work on marginal failures caused by slow degradation is justified.

Although individual elements within a FLO device will fail separately, the elements are fabricated in a batch process which results in complex interrelations. For example, if a Pyre-M.L. tube is too long, the plated conductor areas over the tube edge might be very thin. Because of the interrelations, tests on individual elements of the device must be made on samples that are very similar to those that will be included in the eventual FLO structure. This also implies that the fabrication process must be relatively stable when these tests are performed. Failure modes in the ferrite tend to be independent of the dielectric and conductor failures, so that complete devices need not be fabricated in order to evaluate new methods for fabricating the dielectric/conductor system.

Failure by degradation should receive the main emphasis in the reliability prediction of a complete FLO system because catastrophic failures will have been reduced to a low level before such a prediction would be meaningful. For example, the gradual extension of a crack in the ferrite will cause changes in the device characteristics resulting in narrower and narrower operating margins as the flaw increases in size. A conductor which changes resistance due to aging would have similar effects on the system. The FLO system analysis, therefore, is concerned with setting reasonable tolerances on the individual elements so that failures due to degradation will be minimized. Catastrophic failures will almost always result in system failures and are, therefore, much less difficult to analyze.

B. Reliability Diagram for the FLO Device

There is no redundancy imbedded in the FLO device, so the series logic model* is the appropriate one to use to represent device reliability. This means that the failure of any one of the several items is sufficient to cause the failure of the entire device. In the reliability diagram, Figure 30, each rectangle is to be interpreted as constituting an essential part of the entire device (a series item), and a failure of the item in one rectangle causes the device to fail. The rectangles are arranged to represent hierarchical levels; each horizontal group comprises one level. Each lower level represents a more detailed breakdown of the connected rectangle in the level above.

A complete breakdown of all failure modes to the level of the smallest reliability item becomes too detailed to present in one small diagram. An example in Appendix B gives a detailed breakdown of drive windings shorted by way of the shield and shorted within a Pyre-M.L. tube.

C. Accelerated Testing of Ferrite

With the fabrication techniques employed so far for FLO devices, the catastrophic failure rate has been unacceptably high. The accelerated tests were therefore simplified because frequent monitoring of variables has not been required in most cases.

Improvements in ferrite technology, however, are expected, and simple tests could be used to evaluate the improvements in ferrite independent of improvements in the dielectric/conductor system. Modifications or improvements in the ferrite may also require different logic structures, but these can probably be evaluated independent of the method used for evaluating the dielectric/conductor system. The most sensitive test for

---

*Appendix A.

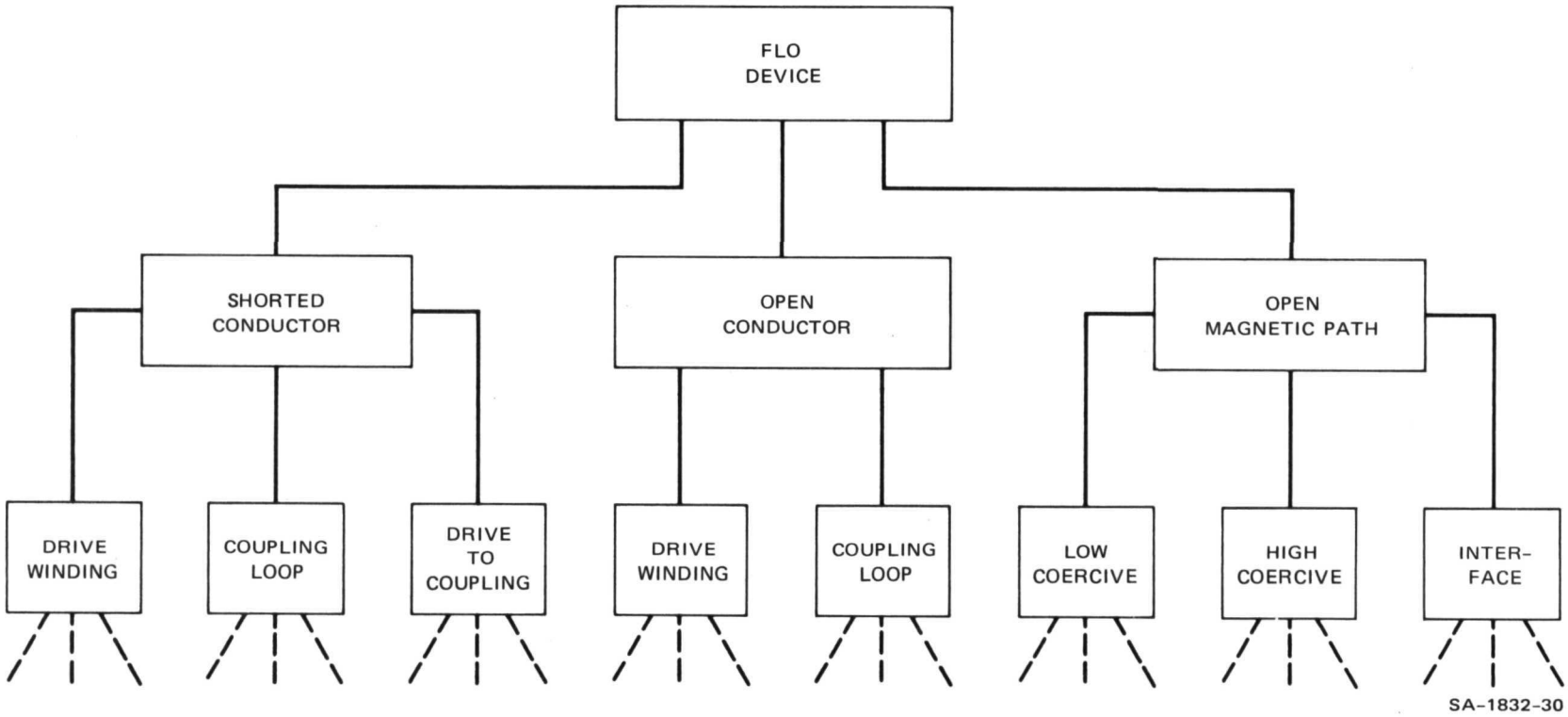

FIGURE 30 DEVICE RELIABILITY DIAGRAM

accelerated aging of the ferrite is temperature cycling. Vibration, in addition to the temperature cycling, should also be useful but is believed to be secondary in importance at this time in the development, since the vibration sensitivity of the devices is so dependent on the dielectric/conductor system chosen and on the details of the methods of mounting the complete assembly.

Following the accelerated test, or from time to time during the test, magnetic measurements can be made with fair sensitivity to indicate whether or not the ferrite structures are stable. The most sensitive test, however, is probably metallurgical-type examination of the ferrite after extended cycling. This procedure is carried out either by lapping and polishing surfaces, or by metallurgical sectioning, and subsequent microscopic examination.

If a ferrite process looks promising, it is then worthwhile to add the first layer of FLO structure, namely the eddy current shield.

D. Tests on Conductor/Dielectric Systems

Unlike the ferrite structure of a FLO device, the dielectric and conductor systems for new development should be tested together. Almost all proposed improvements to the FLO dielectric/conductor structure are related to the process of delineating the conductor pattern on a previously deposited dielectric. For example, the use of vapor-deposited Parylene dielectric has been suggested. If Parylene were used, the conductor pattern could be delineated by either a striping process, as in the present FLO technology, or by a photo-resist process. In either event, a complete assembly using similar thicknesses, radii of curvature, conductor spacing, and conductor width would have to be used to closely simulate the dielectric/conductor structure used in the FLO device. The cost of fabricating and testing samples of the dielectric/conductor

technology would, however, be only a fraction of the cost of fabricating and testing completed FLO units. Testing of a new dielectric/conductor technology independent of the exact FLO configuration would also allow extrapolation of the test results to other interconnection systems, such as the interconnection of semiconductor devices.

The most useful tests for dielectric/conductor systems are:

(1) Temperature cycling

(2) Soak at a high temperature

(3) High humidity at moderate temperature.

The use of vibration tests is not particularly meaningful until the complete assembly, including ferrite and mounting hardware, is available.

The conductor test pattern can be designed so that it is very easy to detect changes in resistance or dielectric characteristics. Properly designed test patterns allow more accurate measurements of the basic parameter changes than is possible in completed FLO devices.

VIII TEST EQUIPMENT AND PROCEDURES

A variety of equipment, some of it highly specialized was used for the experiments and measurements carried out during this project. Most of the equipment was available and ready for use as a result of previous project work; no special equipment was purchased or developed on this project.

A. Magnetic Device Characteristics

Three specialized pieces of laboratory equipment have been used to measure the magnetic characteristics of multipath ferrite structures and of completed test specimens. These were designed and constructed at SRI several years ago to facilitate performance of research on all-magnetic logic devices and systems.

A "Laboratory Pulser" provides current pulses of varying widths, amplitudes, and repetition rate from a high impedance source. It has ten output channels, each of which has a maximum pulse amplitude of 4.5 amperes. The pulse width is adjustable from a few microseconds to several milliseconds, and there are ten time phases available for each of the ten output channels. This equipment is suitable for performing a variety of tests on multipath ferrite cores and on magnetic circuits.

A second specialized piece of equipment is a "Semiautomatic Static φ-F Plotter." As the name implies, it is used for measuring the static φ-F (switched flux versus applied magnetomotive force) characteristic on ferrite multipath cores. (It can also be used on ferrite toroids, which are single-path cores.) The equipment switches a controlled amount of flux in a specified magnetic path during a 30 ms interval. At the end

of this time, the path is saturated in a cyclic manner by three 10 μs current pulses. The 30 ms duration is long compared to the switching time of ferrite cores, so quasi-static characteristics are measured.

When accurate levels of switched flux were measured, a "Flux Reference" was used. This equipment facilitates making measurements that are independent of such factors as amplifier gain and therefore can be used to measure the stability of parameters in a test specimen over a long period of time. The smallest flux unit that can be measured with this equipment is 3.6 nWb. This rather unusual unit is determined by the flux switched in a toroid within the equipment.

B. Temperature Stressing

Temperature chambers controlled by a timer were used to cycle the ambient temperature of test specimens and to soak at temperature. We used them over the range of -55° to +150°C on this project.

In order to cycle the temperature of a test specimen more rapidly than is possible with conventional test chambers, we devised a configuration composed of heat lamps, a blower, and a timer. With this arrangement, a test specimen can be cycled 144 times from room temperature to +150°C in a 24-hour period. A platinum resistance temperature sensor, an infrared sensor, and thermistors were used for temperature measurement.

C. Humidity Exposure

The means used for controlling the ambient humidity was simple but effective. Specimens were placed in a desiccator chamber with either a desiccant or water-saturated cotton controlling the humidity. The specimens were isolated from the desiccant and the water per se. After allowing for a period of stabilization of the humidity with specimens in the chamber, the specimens were removed briefly from the chamber for measurements and observation.

D. Vibration Stressing

The vibration stressing of a test specimen was done after first securing the specimen to a metal plate using RTV Silastic. This rubber compound was placed in contact with the edges of the multipath ferrite cores as well as the Kapton because the cores comprise most of the mass of the specimen. Because the test specimens weigh only 1.2 grams, a small shaker is adequate. The force rating on the one we used is 29 Newtons (6.6-pounds force).

E. Microscopy

A variety of microscopes have been used for visual study of the test specimens. For high magnifications a metallographic-type microscope was used. With this microscope, magnifications up to 1000× are possible without oil immersion (although better quality is obtained at 1000× with oil immersion). Various filters and lighting controls are integral to this equipment.

In preparing a specimen for examination under high magnification, it is first immersed in a casting compound under a vacuum so that voids are filled and essential device features preserved. Following this, the specimen is either ground and polished, or cut in pieces with a diamond saw and then ground and polished.

F. Miscellaneous

A variety of miscellaneous equipment was used in addition to that mentioned above, including special photographic facilities, a metal hardness tester, and a megohmmeter measuring with the applied voltage controllable from 50 to 500 volts.

REFERENCES

1. D. R. Bennion and H. D. Crane, "All-Magnetic Circuit Techniques," Advances in Computers, Vol. 4, 1963, p. 53-133.

2. C. H. Heckler, Jr. and N. C. Bhiwandker, "Development of Magnetic Logic Batch Fabrication Techniques," Report RR 70-04, Ampex Corporation, Redwood City, California, Contract NAS1-7878, NASA CR-66890 (1970).

3. C. H. Heckler, Jr. and N. C. Bhiwandker, "Batch Fabrication Process Development for Ferrite Logic Conductors," Report RR 71-15, Ampex Corporation, Redwood City, California, Contract NAS1-9836, NASA CR-111983 (1972).

4. C. H. Heckler, Jr., "Development of Ferrite Logic Devices for an Arithmetic Processor, "Report RR 72-22, Ampex Corporation, Redwood City, California, Contract NAS1-10816, NASA CR-112198 (1972).

5. D. R. Bennion, D. Nitzan, and H. D. Crane, Digital Magnetic Logic, McGraw-Hill Book Co., New York, N.Y. (1969).

6. P. D. Baba and C. H. Heckler, Jr., "Multiple Composition Ferrite Structures," IEEE Trans. on Mag., Vol. MAG-4, No. 3, p. 560 (September 1968).

Appendix A

THEORETICAL MODEL

Appendix A

THEORETICAL MODEL

The failure of a FLO system to operate as specified, or failure of an electrical system in general, can result from both catastrophic and degradation failures. Furthermore, degradation type failures can lead to catastrophic failures. In the discussions that follow, we shall not distinguish between these two types of failures. Instead, we shall distinguish between the reliability of a single item or element and the reliability of an entire system.

1. Reliability of a Single Item

The effects of modes of failure, time, tolerance, environment, and stress versus strength on the reliability of a single item are discussed below.

a. Mode of Failure

Suppose that an item may be in either a successful operating state, S, or in one of k failure states, F_j, where j = 1,2,... k. Then

$$R = \text{Prob}(S) = 1 - \sum_{j=1}^{k} \text{Prob}\left(F_j\right) \quad . \tag{1}$$

For example, k = 1 for a wire (open), k = 2 for a diode (short, open), and k > 2 for a transistor.

b. Effect of Time

If f(t) is the probability density function (pdf) of failure versus time, then the probability of failure

$$F(t) = \int_0^t f(t)dt \tag{2}$$

increases with time, and the reliability

$$R(t) = 1 - F(t) = \int_t^\infty f(t)dt \tag{3}$$

decreases with time.

The hazard function is defined as

$$h(t) = \frac{f(t)}{R(t)} \quad . \tag{4}$$

The Weibull pdf,

$$f(t) = \beta \lambda t^{\beta-1} e^{-\lambda t^\beta} \tag{5}$$

has two parameters, β and λ. If $\beta = 1$, Eq. (5) is reduced to the exponential pdf

$$f(t) = \lambda e^{-\lambda t} \tag{6}$$

and following Eqs. (3) and (4),

$$R(t) = e^{-\lambda t} \tag{7}$$

and $h(t) = \lambda$ = constant, which is also the failure rate.

The pdf of the bathtub-shaped h(t) is

$$f(t) = \sum_{j=1}^{3} \text{Prob}\left(F_j\right) f_j(t) \qquad (8)$$

where j = 1,2,3 correspond to failure during the decreasing h(t) ("burn-in" period), constant h(t) ("useful life" period), and increasing h(t) ("wear-out" period), respectively (see sketches below). Each pdf f_j can be described by Eq. (5): $\beta < 1$ for j = 1, $\beta = 1$ for j = 2, and $\beta > 1$ for j = 3.

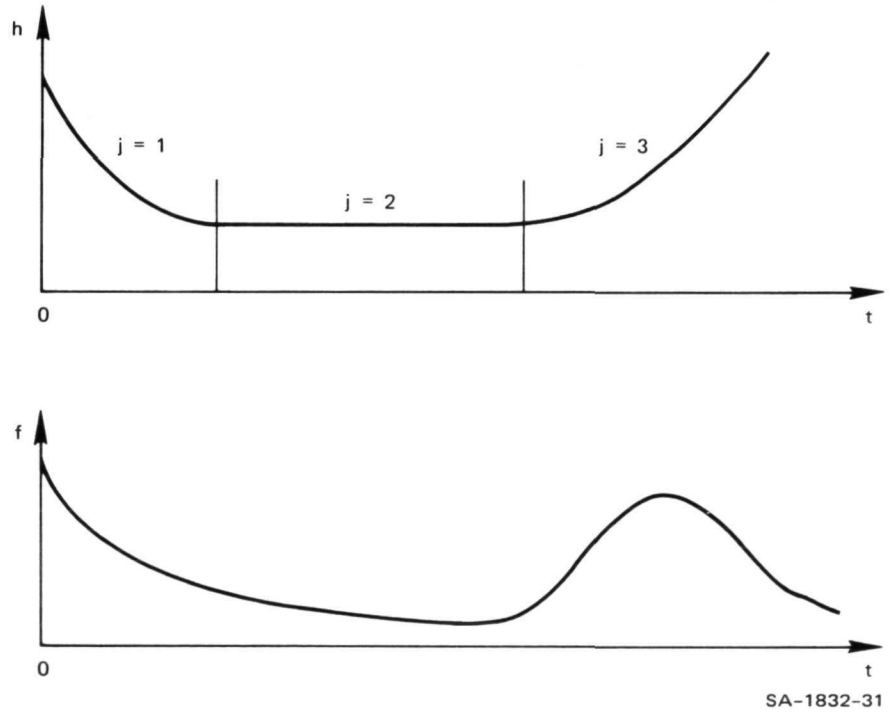

c. Performance Tolerance

Failure (catastrophic or degrading) may occur if the performance strength, y, is out of the operation region $y_{min} \leq y \leq y_{max}$. Thus,

$$R = \text{Prob}\left(y_{min} \leq y \leq y_{max}\right) \quad . \qquad (9)$$

If p(y) is the pdf of y, then

$$R = \int_{y_{min}}^{y_{max}} p(y)dy \quad . \tag{10}$$

Example: Coupling-loop resistance, R_{ℓ}, will vary from one device to another. If the resistance lies between some minimum value, $R_{\ell min}$, and a maximum value, $R_{\ell max}$ (see below) the device will operate satisfactorily.

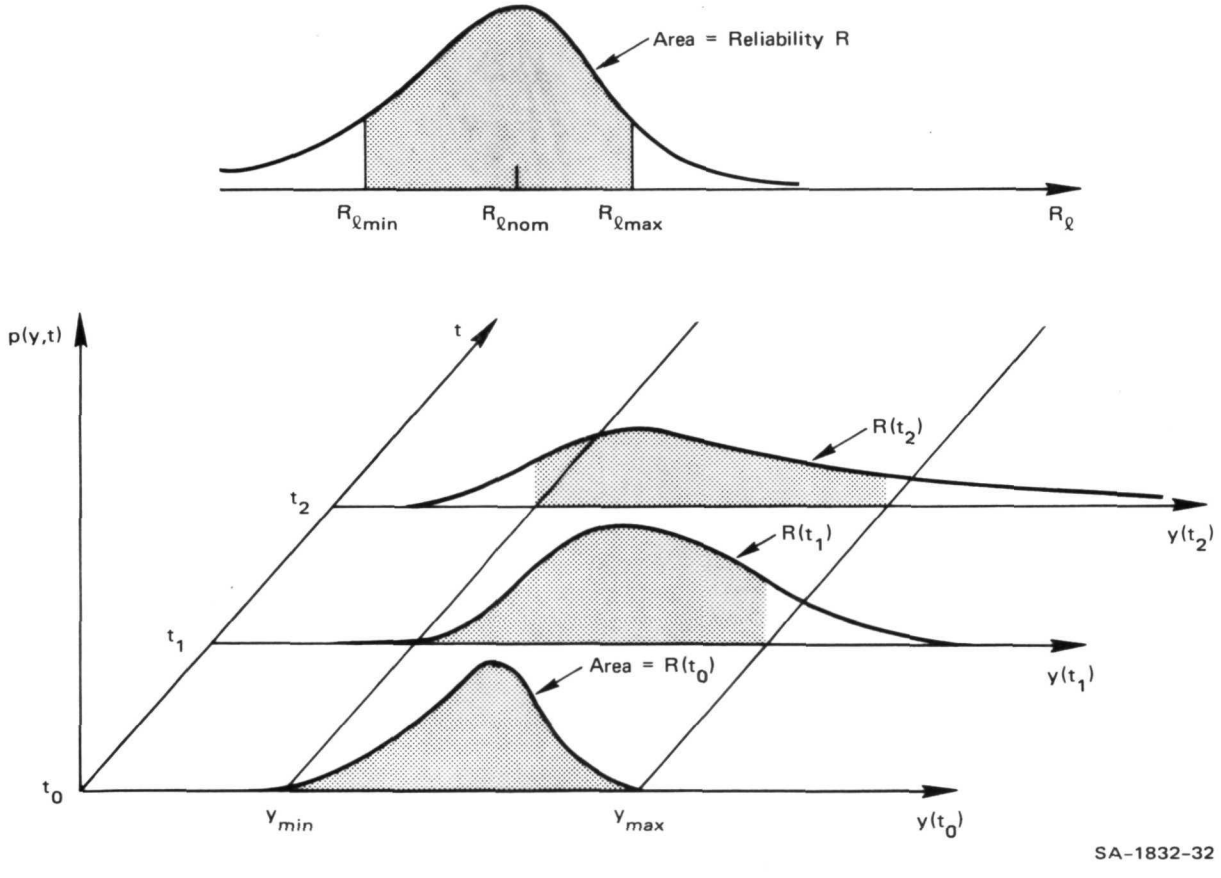

If p(y) varies in time, then p = p(y,t) and R = R(t), as illustrated in the sketch. The reliability expression then becomes

$$R(t) = \int_{y_{min}}^{y_{max}} p(y,t)dy \quad . \tag{11}$$

d. Effect of Environments

Let E_i designate the event of an ith environment among k possible environments, i.e., E_1, E_2, ... E_k are mutually exclusive and exhaustive events (of which one necessarily occurs). If Prob(No F/E_i) is the probability of no failure by time t under environment E_i, then the reliability (of no failure by time t) is

$$R = \sum_{i=1}^{K} \text{Prob}\left(\text{No } F/E_i\right)\text{Prob}\left(E_i\right) \quad . \tag{12}$$

For a random environment which is continuous,

$$R = \int_E \text{Prob(No } F/E)p(E)dE \tag{13}$$

where p(E) is the pdf of E.

e. Effect of Strength versus Stress

Let s designate the environment stress such that failure occurs if $s > y$, where y is the performance strength. Thus, the reliability is

$$R = \text{Prob}(y > s) = \int_0^{\infty}\left[\int_s^{\infty} p(y)dy\right]p(s)ds \tag{14}$$

where p(s) is the pdf of the stress. Note the analogy between Eqs. (13) and (14), since $\int_s^\infty p(y)dy$ is the probability of no failure for given stress s, shown below

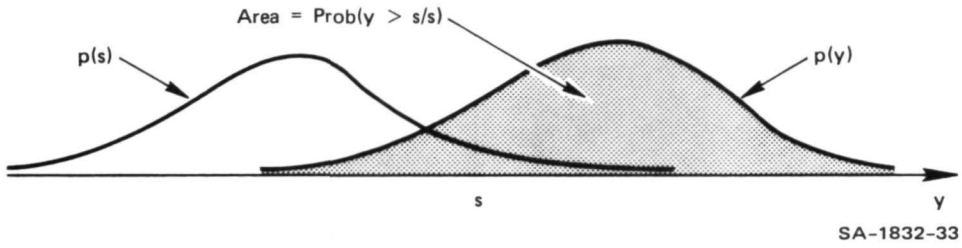

Suppose that both p(s) and p(y) are normally distributed with (mean, standard deviation) of (μ_s,σ_s) and $\mu_y,\sigma_y)$, respectively. Hence, y-s is distributed normally with mean $\mu_y - \mu_s$ and standard deviation

$$\sqrt{\sigma_y^2 + \sigma_s^2} \quad .$$

Thus,

$$R = \text{Prob}(y > s) = \text{Prob}(y - s > 0) = 1 - \Phi\left[\frac{-(\mu_y - \mu_s)}{\sqrt{\sigma_y^2 + \sigma_s^2}}\right] \qquad (15)$$

where Φ (a) = Prob(x > a) and where x is distributed according to the standard normal distribution.

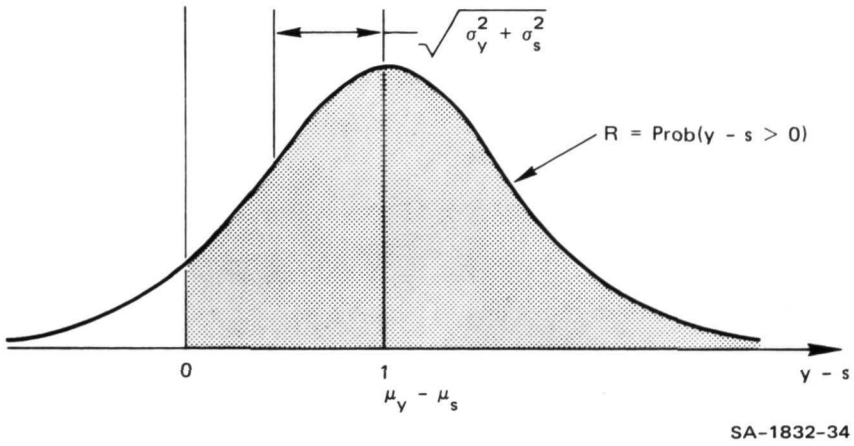

2. Reliability of a Multi-Item System

The reliability of each item in a system is evaluated by the methods described in Section 1. Given item reliabilities, there are several methods to calculate the reliability of a system consisting of these items. Here we discuss only one method, namely the "logic models" method, and then examine the effect of time on this method.

a. Logic Models

A logic model treats each item of a system as an item (gate) of a logic circuit. Let

$$R_j = P\left(I_j\right) \tag{16}$$

be the reliability of the jth item of a system, i.e., the probability of no failure of Item I_j.

We distinguish among series logic, parallel logic, and mixed series-parallel logic models, as follows.

(1) Series Logic Model

The model consists of n items, I_1, I_2, ... I_n shown in series in the sketch.

SA-1832-35

Failure occurs if at least one item fails. If the reliabilities R_j's are independent, then the reliability of the series-model system is

$$R = \prod_{J=1}^{n} P\left(I_j\right) \tag{17}$$

If the R_j's are dependent, then R is a conditional probability, i.e.,

$$R = P\left(I_1\right)P\left(I_2/I_1\right)P\left(I_3/I_1I_2\right)\ldots P\left(I_n/I_1I_2\ldots I_{n-1}\right) \tag{18}$$

Note that Eq. (18) reduces to Eq. (17) if the $P(I_j)$'s are independent.

Let the probability of failure of the ith item be denoted by

$$Q\left(I_j\right) = 1 - P\left(I_j\right) \tag{19}$$

If all the items are identical, then $P(I_j) = P(I)$ and Eq. (17) is reduced to

$$R = P^n(I) = [1 - Q(I)]^n \quad . \tag{20}$$

Expanding $[1 - Q(I)]^n$ as Taylor series, and since it is likely that $Q(I) \ll 1$, then

$$R \approx 1 - n\,Q(I) \quad . \tag{21}$$

(2) Parallel Logic Model

The model consists of n items, I_1, I_2, ... I_n, in parallel. This is represented in circuit form as follows:

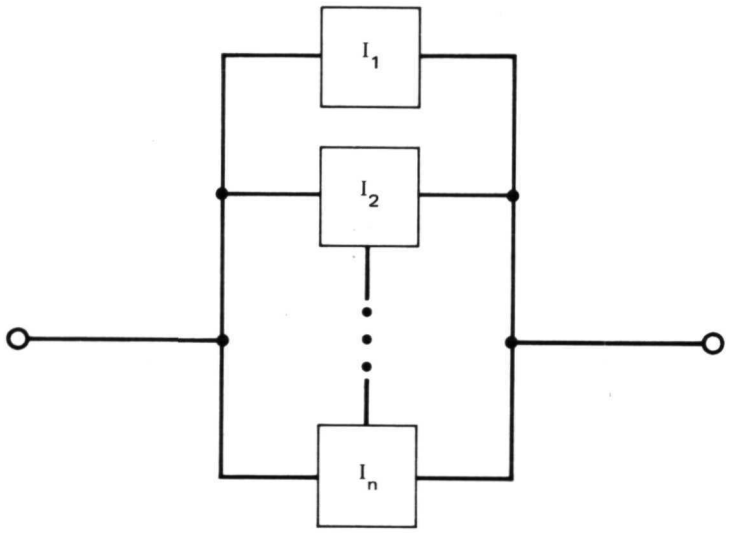

SA-1832-36

Failure occurs if all n items fail, implying that this model is useful for a system employing redundancy to increase reliability. If R_j of each item is independent, then

$$R = 1 - \prod_{j=1}^{n} Q\left(I_j\right) \quad . \tag{22}$$

If the R_j's are dependent, then

$$R = 1 - Q\left(I_1\right)Q\left(I_2/I_1\right)Q\left(I_3/I_1I_2\right)\ldots.Q\left(I_n/I_1I_2\ldots I_{n-1}\right) \quad . \tag{23}$$

If the items are identical and independent, then $Q(I_j) = Q(I)$ and Eq. (22) is reduced to

$$R = 1 - Q^n(I) \quad . \tag{24}$$

If at least k of these n identical independent items must fail in proper operation, then

$$R = \sum_{i=k}^{n} \binom{n}{i} P^i(I)\, Q^{n-i}(I) \quad . \tag{25}$$

Note in Eq. (25) that $\binom{n}{i} P^i(I)\, Q^{n-i}(I)$ is the probability that any i items of the n items have not failed and that (n - i) items have failed. Since the system operates properly if $k \leq i \leq n$, this probability is summed from i = k to i = n.

(3) Mixed Series-Parallel Logic Model

The model consists of s subsystems in series, each of p_i items in parallel. This can be represented as a combination of parallel and series circuit elements.

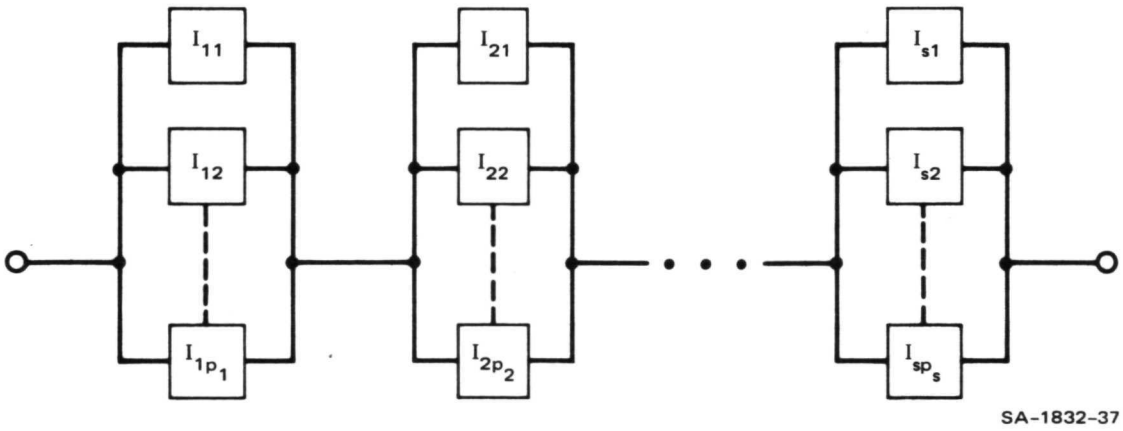

Using (2.7), the reliability of the ith subsystems S_i is

$$P(S_i) = 1 = \prod_{j=1}^{p_i} Q(I_j) \quad . \tag{26}$$

Substituting Eq. (26) into Eq. (17), the reliability of the entire system is

$$R = \prod_{i=1}^{n} \left[1 - \prod_{j=1}^{p_i} Q(I_j) \right] \quad . \tag{27}$$

b. Effect of Time

The effect of time may be introduced into the logic models by simply replacing $R_j = P(I_j)$ of Eq. (16) by

$$R_j(t) = P(I_j, t) \quad . \tag{28}$$

For convenience, let us use the exponential pdf of Eq. (6) for each jth item, i.e.,

$$f_j(t) = \lambda_j e^{-\lambda_j t} \tag{29}$$

where λ_j is the failure rate of the jth item. Following Eq. (7),

$$R_j(t) = P(I_j, t) = 1 - Q(I_j, t) = e^{-\lambda_i t} \quad . \tag{30}$$

We now apply Eq. (15) to the various logic models, assuming independent λ_j's.

(1) Series Logic Model

Applying Eq. (30) to Eq. (17),

$$R(t) = \prod_{j=1}^{n} e^{-\lambda_i t} = e^{-\lambda_s t} \tag{31}$$

where

$$\lambda_s = \sum_{j=1}^{n} \lambda_j \quad . \tag{32}$$

Thus, the failure rate of a series logic model is the sum of the failure rates of the individual items.

(2) Parallel Logic Model

Applying Eq. (30) to Eq. (7),

$$R(t) = 1 - \prod_{j=1}^{n} \left(1 - e^{-\lambda_j t}\right) \quad . \tag{33}$$

If $\lambda_i t \ll 1$, then

$$I - e^{-\lambda_j t} = 1 - \left(1 - \lambda_j t + \frac{\left(\lambda_j t\right)^2}{2!} - \ldots\right) \cong \lambda_j t$$

and Eq. (33) is simplified to

$$R(t) \cong 1 - \lambda_p t \tag{34}$$

where

$$\lambda_p = \prod_{j=1}^{n} \lambda_j \quad . \tag{35}$$

Thus, if $\lambda_j t \ll 1$, the failure rate of a parallel logic model is approximately the product of the failure rates of the individual items.

(3) Mixed Series-Parallel Logic Model

Applying Eq. (30) to Eq. (27),

$$R(t) = \prod_{i=1}^{n} \left[1 - \prod_{j=1}^{p_i} \left(1 - e^{-\lambda_j t} \right) \right] \cong \prod_{i=1}^{n} \left(1 - t \prod_{j=1}^{p_i} \lambda_j \right) \quad . \tag{36}$$

Appendix B

AN EXAMPLE SHOWING A DETAILED DIAGRAM FOR SHORTED CONDUCTORS

Appendix B

AN EXAMPLE SHOWING A DETAILED DIAGRAM FOR SHORTED CONDUCTORS

The diagram shown in Figure B1 illustrates a method that can be used to divide the reliability items in greater detail than was done in Figure 30. The representation used in this detailed diagram is an extension of that used earlier. Each of the small boxes containing a class number, defined below, is to be treated as a unit that can cause or contribute to the shorting mode described in the connected rectangle above. This extension to the earlier representation is necessary because one short is sometimes insufficient to cause device failure. For example, if a drive winding shorts to a shield at one and only one place, the device remains operative. If two different windings each short to the same shield, the device fails. If two different segments of the same winding each short to a shield, the device usually fails (shorted turn), depending upon the class of segments involved.

Consider the rectangular box labeled "Class I" that is connected to the box labeled "Two Segments to ODD Core." A short of any two of these segments would result in a failure. A failure would also result when only one of these segments is shorted and simultaneously a segment from the box labeled "Class II" is also shorted to the shield. The Arabic numeral in each box indicates the number of that class of segments that can fail by the mode given in the connected box above. The reliability of each segment within a box is assumed to be the same as each other segment in that same box.

Under some circumstances, there is a small inaccuracy introduced by using the numeral given in a box. For example, if a Class I segment and

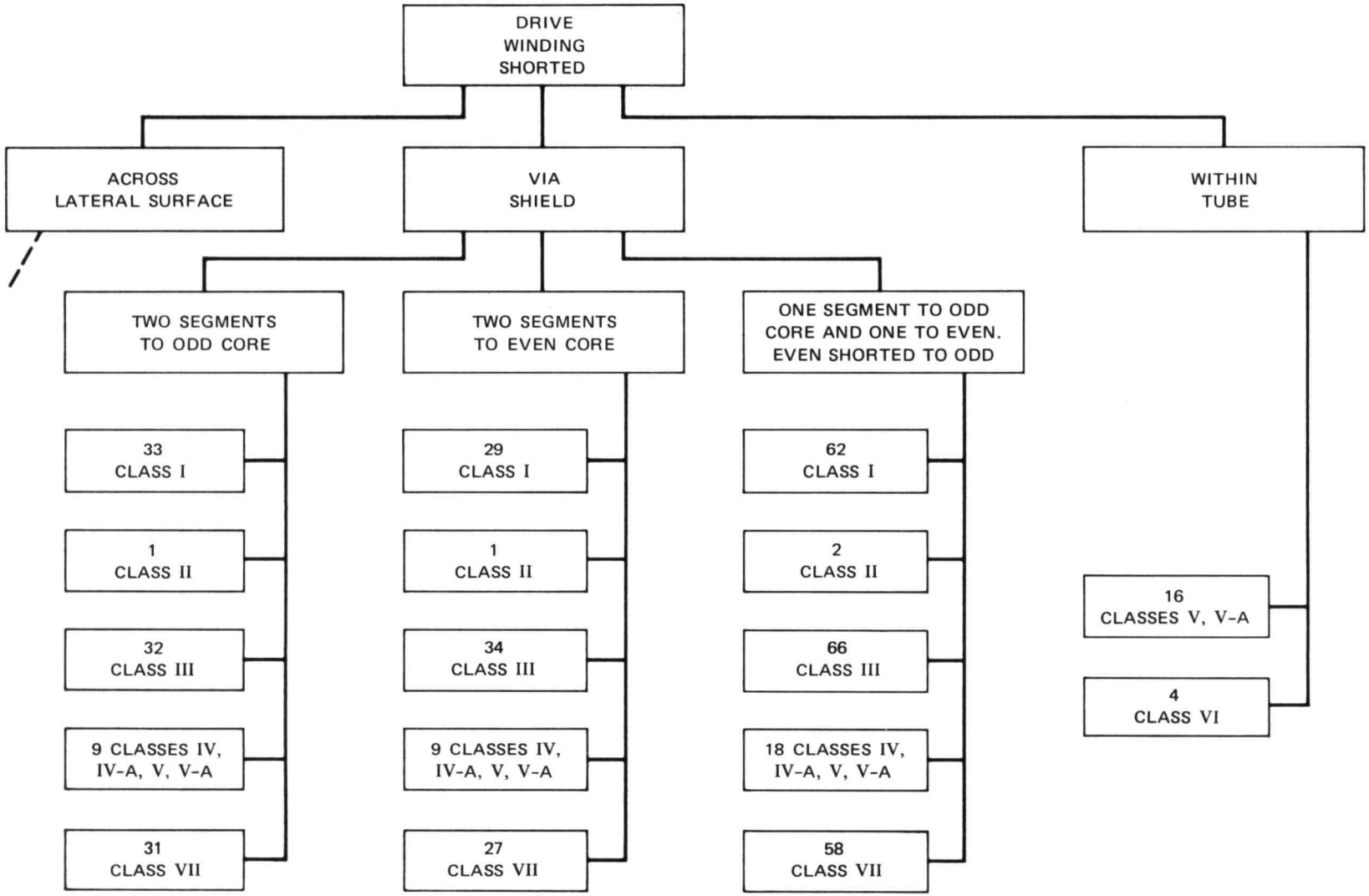

FIGURE B1 DRIVE WINDING EXAMPLE

a Class VII segment are both shorted to the same shield, and if these two segments are contiguous to each other, then the shorts merely provide a parallel conducting path for a short distance, and the device would remain operative. In circumstances such as this one, the number of possible combinations of shorts that causes device failure is the number indicated in the box reduced by one. To carry an analysis to this degree of rigor is unwarranted at this stage of device development. The segment enumeration given in the figure was carried out on the basis of the early configuration of conductor paths and tube placement. Since that time, some slight modifications have been in the geometry of some conductor segments. Furthermore, the precise number of segments of a given class is subject to the judgment of the person analyzing the geometry of the conductors, because a few segments are borderline cases and could be classified in either one of two possible classifications. For the purposes of demonstration, the numerals given in the diagram are adequate.

For the drive windings and coupling loop conductor paths, one can make two broad classifications. The first comprises paths that are lateral (on the surface of the Kapton and/or epoxy), and the second comprises vertical paths (through tubes). Within these two broad classifications there are many distinctive features that lead to more detailed classification. We define a lateral segment as a conductor portion on the lateral surface of the device that is terminated on one end (only) by a Pyre-M.L. tube. This definition requires, in general, that another lateral segment shall terminate the segment end that is not terminated at a tube. The exception to this generality is the termination of a lateral segment by a drive winding connection tab (the tab for connection to a laboratory pulser).

A vertical segment is, by definition, inside a Pyre-M.L. tube; it traverses the entire tube length. All the vertical segments of the drive windings are essentially the same length, while the lateral segments vary

considerably in length. The vertical segments of the coupling loop are greater in length than are those of the drive windings. This definition of vertical and lateral segments means that there are twice as many lateral segments as there are vertical segments.

The following is a listing of the segment classes that we have defined for the FLO device. The first seven classes refer to the drive windings and the remaining four classes refer to the coupling loop. Only drive windings are included in Figure B1.

Drive Winding Segments

- Class I--A lateral segment upon epoxy and Kapton surfaces and overlaying the eddy current shield.
- Class II--A lateral conductor upon epoxy and Kapton surfaces, the Kapton not supported by underlaying ferrite.
- Class III--A lateral segment upon epoxy and Kapton surfaces and overlaying the unshielded surface of the ferrite (same as Class I except there is no shield underlaying).
- Class IV--A vertical segment in a Pyre-M.L. tube within an aperture in the multipath ferrite.
- Class IV-A--Same as Class IV except that an additional Pyre-M.L. tube (for the coupling loop) is inside the tube/conductor structure.
- Class V--A vertical segment within a tube wherein there is another vertical segment in the same tube, and the tube is within an aperture of the multipath ferrite.
- Class V-A--Same as V except that an additional Pyre-M.L. tube (for the coupling loop) is inside the tube/conductor structure.
- Class VI--A vertical segment in a Pyre-M.L. tube that is inside a clipper toroid-pair (there are two segments in each tube).
- Class VII--A single vertical segment in a tube wherein the tube is not in an aperture of the multipath ferrite device or a toroid pair, i.e., the tube is not surrounded by ferrite, but part of the tube is adjacent to shielded ferrite.

Coupling Loop Segments

- Class VIII--A lateral coupling loop segment that overlays epoxy, or overlays epoxy and Kapton surfaces.
- Class IX--A vertical coupling loop segment in a tube in an aperture of the multipath ferrite.
- Class X--A vertical coupling loop segment in a clipper toroid-pair.
- Class XI--A vertical coupling loop segment that passes through an aperture in the multipath ferrite wherein there is a second coupling loop segment in the same Pyre-M.L. tube.

DISTRIBUTION LIST

ORGANIZATION	NO. OF COPIES
NASA Langley Research Center Hampton, VA 23665	
Attn: Report & Manuscript Control Office, Mail Stop 180A	1
Raymond L. Zavasky, Mail Stop 115	1
Dale G. Holden, Mail Stop 477	25
Technical Utilization Office, Mail Stop 139A	1
NASA Ames Research Center Moffett Field, CA 94035	
Attn: Library, Mail Stop 202-3	1
NASA Flight Research Center P.O. Box 273 Edwards, CA 93523	
Attn: Library	1
NASA Goddard Space Flight Center Greenbelt, MD 20771	
Attn: Library	1
NASA Lyndon B. Johnson Space Center 2101 Webster Seabrook Road Houston, TX 77058	
Attn: Library, Code JM6	1
NASA Marshall Space Flight Center Huntsville, AL 35812	
Attn: Library	1
Jet Propulsion Laboratory 4800 Oak Grove Drive Pasadena, CA 91103	
Attn: Library, Mail 111-113	1
NASA Lewis Research Center 21000 Brookpark Road Cleveland, OH 44135	
Attn: Library, Mail Stop 60-3	1

ORGANIZATION	NO. OF COPIES
NASA John F. Kennedy Space Center Kennedy Space Center, FL 32899	
Attn: Library, IS-DOC-1L	1
National Aeronautics & Space Administration Washington, DC 20546	
Attn: KSS-10/Library	1
REI/NASA Headquarters	1
Advisory Group on Electronic Devices 201 Varick Street New York, NY 10014	
Attn: Mr. Warner Kramer	1
Commanding General, U.S. Army Electronics Command Fort Monmouth, NJ 07703	
Attn: AMSEL-TL-MA, Mr. T. S. Gore, Jr.	1
Air Force Materials Laboratory Wright Patterson, OH 45433	
Attn: Mr. Jules I. Wittebort, LTE	1
Director Naval Research Laboratory Washington, DC 20390	
Attn: Dr. Lawrance R. Whicker, Code 5250	1
Department of the Air Force Headquarters Rome Air Development Center (AFSC) Griffiss Air Force Base, NY 13440	
Attn: RCRS, Mr. L. J. Gubbins/330-4064	1
NASA Scientific & Technical Information Facility P.O. Box 33 College Park, MD 20740	12 (plus reproducible)